

1 Dear Editor,

2 Thank you very much for the re-evaluation of our manuscript. We adapted it according to the
3 comments and are certain it will be accepted in the updated version.

4 We extended the description of the original thermal maturity data and their cross-correlation,
5 extended the section on upper thermal boundary condition of the basin model and changed the
6 figures and tables as suggested.

7 The discussion part in which we compare our data with published data by one of the reviewers was
8 again adapted according to his comments. Our data set comprises different, independent
9 thermometers which are in accordance with other published data but do not agree with the results of
10 Aldega et al. We now wrote in our discussion: "At present, there is no clear explanation for this
11 discrepancy". We included some possible explanation for it but can't solve this discrepancy. Future
12 discussions we would prefer to continue in literature, to allow the scientific community to fully take
13 part in it.

14 We hope that after these modifications the manuscript can be accepted.

15 With kind regards,

16 Arne Grobe

17 Dear Authors,

18 Thanks for the revision of the manuscript.

19 Your revised version was reviewed by the previous reviewers (Rev#1 and Rev#2) and by a new one
20 (Rev#3). Based on their reports and my own assessment, your manuscript has been improved and it
21 is potentially a valuable contribution, but it still needs a further work of revision.

22 Critical issues deal with (i) the thermal structure and boundary conditions assumed for the basin
23 modelling (Rev#3) and (ii) (still) the thermal maturity data, their cross-correlation and interpretation
24 (Rev#2). These points are essential to better constrain and support the tecto-thermal evolution of the
25 continental margin. On this regard, both reviews provide an effective guide to prepare a suitable
26 revised version of the manuscript.

27 I would also suggest to place in the main text some of the representative T-t paths as obtained from
28 the forward modeling of the thermochronology data. Some details are necessary to better illustrate
29 the T-t modeling results of the different units shown in S4 and S5: which the boundary conditions?
30 what relevant for the tectono-thermal evolution of the continental margin? Did the T-t forward
31 modeling presented in S4 and S5 take into consideration also the available thermochronological data
32 set shown in Figure 3? All these points are critical when discussing the "burial" and "exhumation
33 history" in sections 5.1 and 5.2 and should be integrated in the burial/exhumation history of the
34 continental margin presented in Figure 12 (that actually does not only describe the burial history as
35 stated in the Figure caption of Figure 12, but also the exhumation history). In other words, Figure 12
36 (and the related text, lines 597-604) is the synthesis of the entire data set, which should also take into
37 consideration the thermochronological data (exhumation history). See also comments from Rev#2 on
38 this regard.

39 As suggested we updated Figure 12 and its caption and rephrased the related discussion to highlight
40 the integration of all datasets in this Figure. Regarding the models in Figures S4 and S5, as each of the

41 T-t forward models is based on one single sample we did not include it in the main manuscript as it is
42 not adding much value.

43 Since the amount of required revision is significant, I am returning back your manuscript with a
44 decision of major revision.

45 When submitting a revised version, please also include a "Author's response file" that lists changes
46 and describes how the manuscript has/has not been modified following the Reviewer's comments.

47 Looking forward for a suitable revised version,

48 sincerely,

49

50 Federico Rossetti

51

52 2nd Review Solid Earth

53 Referee 1 Massimiliano Zattin – Accept as is – no further comments

54 Referee 2 Luca Aldega - **major revision**

55 This revised version of the manuscript shows an improved organization of the text. Main weakness
56 about explaining the importance of the paper and its scientific significance for the Solid Earth
57 audience has been solved. However, there are still a few points that need further details or should
58 be considered.

59 1) I do not see too much improvement about describing solid bitumen data. Still there are only four
60 lines for presenting original data and this seems to me too little when compared with fluid inclusion
61 and thermochronology chapters. As solid bitumen data are important for calibrating burial history, I
62 guess that readers would expect some more details. We extended now the cited solid bitumen data
63 in the results section as suggested. Nevertheless, it is on purpose kept shorter than the rest as it is
64 mainly referring to already published data. Moreover, we included the single datapoints in the
65 calibration figure.

66 2) In this manuscript, solid bitumen data are from different stratigraphic units (Sahtan Group,
67 Kharaib Fm., Shu'aiba Fm., Nahr Umr Fm., Natih Fm., Muti Fm.) that cover a long time span from
68 Jurassic to Late Cretaceous. Authors should present their calibrated thermal maturity curve fitting
69 solid bitumen data associated to the 1D burial and thermal models This is actually done in Figures
70 09 and 10, with perhaps unusual presentation of the data, but as maturity values are much higher
71 than in usual sedimentary basins (partly exceeding Easy Ro equations) we needed a solution to
72 adapt the graphics Using the thermal maturity curves by Grobe et al., 2016 that account only for
73 solid bitumen data from the Natih Formation without implementing them with the new data is a
74 missed opportunity to improve and strengthen the model. Moreover, we added a sentence to the
75 discussion that we refined the model of Grobe 2016 with the presented larger dataset.

76 3) I agree with the authors that extensional top-to-NNE shearing might explain that most of the
77 ophiolite units could have been transferred to the Persian Gulf but the southern flank of the Jebel
78 Akhdar dome is also bounded by SW-dipping listric normal faults (see Searle, 2007) that are coeval
79 to extensional top-to-NNE shearing and downthrow ophiolite and Hawasina units against shelf
80 carbonates. Where has all the material coming from the dismantling of 8-10km thick ophiolite
81 overburden gone to the south of Jebel Akhdar dome? We did not observe the by Searle (2007)
82 interpreted SW-dipping listric normal faults as such, but presented a tectonic evolution that
83 interprets these faults as normal to oblique faults in Grobe et al. 2018. This model was discussed
84 with Mike Searle during a visit in 2017 where he agreed with our idea and interpretation. The top-
85 to-NNE shearing would not require erosion of the Ophiolitic nappe but might represent a tectonic
86 thinning of it, therefore an additional sink for erosional deposits is not necessary. This idea is outlined

87 in the text as followed: „Top-to-NNE shearing is associated with tectonic thinning of the ophiolite
88 (Grobe et al., 2018). This tectonic denudation will also result in cooling, and may explain why so little
89 ophiolite is found in the post-obduction sediments. Additionally, ophiolitic material may have been
90 sedimented in the Gulf of Oman.”

91 4) I have already commented part of the discussion in my previous report and the arguments
92 provided in this revision are still questionable.

93 Lines 580-584. Organic matter is more sensitive to temperature changes than clay mineralogy only
94 in hydrothermal/geothermal settings or when the heating event is shorter than 1-2Ma. The burial of
95 the sedimentary succession below the ophiolite (88 to 80 Ma) or the temperature increase prior to
96 exhumation are not the cases. For instance, in the models shown, temperature is higher than 300°C
97 for upper Jurassic rocks from roughly 60 Ma to 50 Ma that is quite long time interval to let both
98 organic and inorganic thermal indicators recording that thermal event. Also the lack of potassium
99 during the evolution of mixed layered minerals cannot be considered as an explanation for the
100 discrepancy between solid bitumen and clay mineral results because carbonate and siliciclastic rocks
101 of similar stratigraphic ages in Aldega et al, 2017 show similar illite content in mixed layers I-S.

102 In contrary to the dominantly temperature-controlled transformation of organic material the clay
103 mineral-based-"thermometers" are sensitive to the availability of potassium. It is known already
104 even from the 60ties, e.g. Reynolds (1963), Srodon (1976), Altaner et al. (1984). In case of a
105 platform limestone environment the basic assumptions/conditions of this methods are not fulfilled,
106 namely the clay mineral transformation requires a siliciclastic bulk composition and pore fluid
107 movement. The bulk lithologies in our study are extremely depleted in siliciclastic components, and
108 the permeability is strongly limited by the compaction and carbonate cement formation (Hunziker
109 et al., 1986). Thus, we do not agree with the argument that the retarded illitization can happen only
110 in short lived hydrothermal systems.

111 Altaner, S.P., Hower, J., Whitney, G., Aronson, J.L., 1984. Model for K-bentonite formation: evidence
112 from zoned K-bentonites in the disturbed belt, Montana. *Geology* 12, 412–415.

113 Hunziker, J.C., Frey, M., Clauer, N., Dallmeyer, R.D., Friedrichsen, H., Flehmig, W., Hochstrasser,
114 K., Roggwiler, P., Schwander, H., 1986. The evolution of illite to muscovite: mineralogical and
115 isotopic data from the Glarus Alps, Switzerland. *Contrib. Mineral. Petrol.* 92, 157–180.

116 Reynolds, R.C., 1963. Potassium-rubidium ratios and polymorphism in illites and microclines from
117 the clay size fractions of proterozoic carbonate rocks. *Goeochimica et Cosmochimica Acta*, 27, 1097-
118 1112.

119 Środoń, J., 1976. Mixed-layer smectite/illites in the bentonites and tonsteins of the Upper Silesian
120 Coal Basin. *Pr. Mineral.* 49 (84 pp.).

121 Lines 586-590. I think that apatite fission track (AFT) data by Saddiqui et al. (2006) could have been
122 misinterpreted. AFT data by Saddiqui et al. (2006) from Vendian and Ordovician rocks (sample 8
123 and 9) have a reset age of 48 and 55 Ma respectively. This means that Vendian and Ordovician rocks
124 should have passed the isotherms 110-120°C of the AFT system (Gleadow and Duddy, 1981) during
125 exhumation at that time and therefore the temperature of the overlying rocks (from upper Jurassic
126 to the Natih Fm) has to be lower than that. During 55 to 48 Ma, most of the burial curves of the 1D
127 models shown in figure 8 intercepts red or green coloured fields indicating that temperature is
128 between 200 and 300°C higher than the reset temperature of the AFT system **Peak Temperatures**
129 **of the Cretaceous layers shown in the Figures intercept indeed yellow to orange colours indicating**
130 **temperatures of 260-310 °C (in accordance with our thermal maturity data).** Elaborating the
131 exhumation time and speed we have to keep all available data in consideration, e.g. Saddiqui et al
132 also states 260 ° between 96 and 70 Ma. Nevertheless, we added a sentence on the possibility of
133 an even quicker exhumation than assumed in the model. Furthermore maximum temperatures
134 experienced by Jurassic rocks in your model are close to or higher than 300°C indicating
135 metamorphic conditions but outcropping rocks are clearly sedimentary. Some clarification is needed.
136 Right, the outcropping rocks are stated in literature as non-metamorphic. However, recent
137 publications and figures therein (Grobe et al. 2018, Tect.) show that Jurassic rocks have experienced

138 ductile deformation. This confirms, that we are reaching a temperature range close to 300 °C
139 (depending on the pressure). We added a reference in the text accordingly.

140 5) figure and tables needs some revision (see points line by line below)
141

142 Abstract

143 Lines 18-19. I would delete these two lines.

144 Lines 21-23. Please state what is the main factor responsible for peak temperature evolution of
145 passive margin units. Obduction? Heat advection? **DONE**

146 Introduction

147 Line 56 – time-temperature history of what? Better specify “of overthrust margins” **added**

148 Tectonic setting

149 Line 126. Replace “constrains” with “constraints” **DONE**

150 Stratigraphic sequence

151 Line 162-163 – Please provide a more detailed description of the Hawasina deposits. Many ZHe ages
152 and some data for deriving peak temperatures for the southern flank of the Jebel Akhdar dome come
153 from Hawasina deposits. Which unit and formation did you analyze? Which lithology? **DONE and we**
154 **added the information of the Fm and Group (which was already included in the table) to the text.**

155 Previous paleothermal data of the autochthon

156 Line 179. Locate “Al Hamra” in figure 1 **DONE**

157 Line 187. Replace “shows” with “show” **DONE**

158 Fluid inclusion thermometry

159 Line 246- Are FI-M1 and 2 quartz or calcite veins? Authors report both compositions in the text. In
160 table 3 the hosting mineral is quartz. Please check it. **As in text and figure we measured quartz**
161 **crystals in quartz rich calcite veins – we double checked consistency in the text**

162 Line 255- delete “sedimentary” before “Hawasina nappe” and “o” before “km” **DONE**

163 Numerical basin modelling

164 Line 298 – What do you mean for “The south of the foothills is unaffected by foredeep”? I would
165 suggest to replace the sentence as follows if it is consistent with authors’ thought: “The area to the
166 south of the Adam foothills is unaffected by foredeep sedimentation” Actually for this area, available
167 paleothermal data are from the Fahud and Natih fields. Please modify the sentence. **Changed as**
168 **suggested**

169 Basin modelling

170 Line 466- replace “at least 4-4.5 km” with “maximum 4 km”. **DONE** Figure 9a and figure 10a should
171 be corrected setting temperature at 140°C for the Jebel Qusaybah area and Ro% at 1.1. For the
172 Jebel Qusaybah area, only data from Mozafari et al., 2015 are available. **DONE**

173 Lines 503-504- provide reference **DONE – we linked our figures accordingly**

174 Burial history

175 Line 529- How can petrographical data constrain the thickness of sedimentary units? I would replace
176 “petrographical” with “geological” **DONE**

177 Lines 533-535. Replace “at least 4 to 4.5 km” with “maximum 4 km”. See comment above. **DONE**

178 Line 542- Replace “was achieved” with “are available” **DONE**

179 Line 555-556. Expand this part. Readers cannot be aware of models by Lutz et al. (2004) Deleted
180 as point was proven by other references already

181 Line 560. Pressure value of 320 MPa calculated from 10 km thick ophiolite units is different from
182 that reported in table 3 (340 MPa). Please revise DONE

183 Line 564-565. What is the mechanism or process that favours the temperature increase prior to
184 exhumation? Heat advection? I would not talk about thermal equilibration. Changed as suggested
185 From your 1D models the temperature increase between maximum burial and exhumation is more
186 than 100°C. Please discuss and provide further details. Extended Furthermore replace "uplift" with
187 "exhumation". DONE

188 Line 575. Replace "mixed illite-smectite layers" with "mixed layers illite-smectite" DONE

189 Line 582. Quantify "burial was short enough" using your modelling results. We did not quantify this
190 as we are not specialized in illite-smectite analyses and its implementation in basin modelling. The
191 sentence is used to illustrate the aforementioned differences between vitrinite and I-S conversion
192 kinetics for which we presented references.

193 Line 592 -64 ± 4 Ma does not mark the time of deepest burial. Please revise. Sentence rephrased
194 to "This exhumation might be a result of the ductile top-to-NNW shearing event (64 ± 4 Ma, Hansman
195 et al., 2018). Its onset marks the exhumation of the carbonate platform after deepest burial."

196 Exhumation history

197 Line 649 – replace "has seen" with "experienced" DONE

198

199 Conclusions

200 Line 695 – is 300°C a burial temperature due to ophiolite obduction or a peak temperature prior to
201 exhumation? "Deepest burial" added

202 Figures and tables

203 Figure 1: locate Al Hamra DONE

204 Figure 2. Replace "white circles" with "black circle" in the figure caption DONE

205 Figure 3. Delete "*" and "+" in front of authors' names in the figure caption. DONE Please enlarge
206 the peak temperature interval of figure 3 in order to contain the error bar of the Fiqa/Muti Fm. DONE

207 Figure 5. Authors could plot also the data for the Natih and Muti Fms. showing the pressure correction
208 needed. Kept as it is to prevent confusion

209 Figure 9a and figure 10 a – The grey area for temperature constraints should be a single line set at
210 140°C as only 1.1 Vr% value (Mozafari et al., 2015) is available for the Jebel Qusaybah area. Modify
211 the text accordingly. DONE

212 Figure 9c. The grey area for temperature constraints should be between 289±3 °C (see table 1)
213 DONE

214 Figure 10c. Grey area derived from calculated VR values (6.69%) is missing in figure 10c (see table
215 1). As described in the caption and the text, standard maturity modelling is limited to a maximum
216 of 4.6, therefore the calibration data is here not shown.

217 Figure 11. Please add temperature and vitrinite-equivalent ranges to the figure intercepting the
218 degree of serpentinization and heat flow variations lines. DONE

219 Figure 12. delete in the figure caption "*" indicate times of overpressure formation" DONE

220 Table 1. Replace "mean Temp." in the last column with "temperature range" as you do not always
221 provide a mean value. DONE Please provide a range of calculated Vr values when they are associated
222 to a temperature range. Why did not you convert bitumen reflectance data by Fink et al., 2015 into
223 calculated Vr values and then into a temperature range? DONE One data is between brackets. Why?

224 Define it in the figure caption. **DONE** Peak temperature ranges for the northern flank of Jebel Akhdar
225 dome in figure 3 are different from those reported in table 1 where a mean value is shown, Please
226 modify values of table 1 accordingly. **Figure 3 shows the measured values and the added +/- 30 °C**
227 **of the calculation errors.**

228 Delete "measured at RWTH" from the reference by Mozafari et al., 2015. **DONE**

229 Table 3. Please replace "sedimentary nappe" with "sedimentary units" or "tectonic units" in the figure
230 caption. A Nappe has a tectonic origin and cannot be associated to sedimentation **Changed to**
231 **Hawasina nappes**

232 -----

233 Reviewer 3 Bruce Levell – minor

I suggest that the authors explain why the sedimentation model used (a prograding delta) for forward modelling the thermal structure of the autochthon is appropriate to the obduction of a cooling slab of ophiolite. Physically this is not intuitive as the ophiolite, initially at least, is a heat source to the top of the autochthon but is here treated purely as a heat sink as kms of sedimented ophiolite at sea water temperatures is heated by a basal heat flow used to tune the temperature structure. The similarity between the two models is in the thermal blanketing effect and the physical argument should be made, at least semi-quantitatively, that this overwhelms other aspects and makes the sedimentation model an acceptable approximation.

We changed text and figures accordingly to avoid misunderstanding. Main focus of the manuscript is the evolution of the passive margin underneath the ophiolite. The rock record clearly shows that the upper parts of the carbonate platform are not heated additionally from above (from a potentially warm ophiolite). We stress the mentioned thermal blanketing in the rephrased text.

In my view the data-rich compilation and new data on the thermal structure of the autochthon is big step forward in understanding the thermal evolution of the Oman Mountains for which I congratulate the authors. **Thank you very much for the valid comment**

234 Point by Point:

235 Line 442-3 "ophiolite obduction reconstructed by rapid, stepwise sedimentation. The ophiolite started off
236 as oceanic crust with a monotonically increasing temperature gradient with depth from 4 deg
237 C at the sea bottom to say 1300 deg C in the asthenosphere. During the obduction process
238 heat would have been lost both from the top by and from the base to the cooler autochthon
239 (perhaps initially 25deg) below. The resulting transient temperature gradient within the
240 ophiolite would have developed to a curve with maximum somewhere near the middle of the
241 nappe and then developed back towards a monotonically increasing temperature with depth
242 to the base, a substantially lower overall temperature towards a steady state gradient
243 governed eventually by the conductivity of the ophiolite. So, over some time period, during
244 the obduction process, the thermal anomaly of the oceanic crust would have dissipated
245 towards a slab with a linear temperature gradient that was reached by progressive cooling. In
246 the subjacent autochthon temperatures would have progressively increased during this
247 whole process at a rate governed by basal heat flow, the heat anomaly of the slab, its
248 thickness, and its conductivity I would expect there to be an additional complication, due to
249 the lateral motion of the slab over the cold autochthon, of a lateral temperature gradient
250 within the slab as the rearward portion of the ophiolite would be obducted over autochthon
251 that was pre-warmed by the leading edge. This is indeed alluded to by the authors
252 observationally on page 21 – **we clarified that we did not use a sedimentation model but that**
253 **we modelled the obduction by rapid emplacement of ophiolitic units. Also the discussion now**
254 **reads: " A regional thermal overprint on the passive margin sediments by warm ophiolite**
255 **obduction can be excluded and is hence not accounted for in the model. Due to the at least 2**
256 **km thick imbricated Hawasina Nappes between the ophiolite and the passive margin**

257 sequence, the thermal overprint did not affect the top of the carbonate platform. Limited
258 thermal overprint of the units underlying the ophiolite is supported by the fact that the
259 sediments of the nappes directly below the ophiolite do not show signs of regional
260 metamorphism in the Jebel Akhdar region (Searle, 1985).” And we added a shorter but similar
261 section to the model methods.

262

263 As far as I can understand in the model used in this work, the ophiolite is either modelled as
264 an advancing sediment wedge, like an extremely rapidly-deposited delta, or essentially
265 instantaneous deposition of sediment over the whole model at one time like a “pelagic rain”.
266 In either model the ophiolite is initially deposited cold (as sediment grains) and so fast that
267 the initial state is close to instantaneous loading ie there is virtually no temperature gradient
268 from surface to base ophiolite. The transient temperature gradient in the ophiolite is then
269 simply one of warming due to the basal heat flow and the thermal blanketing effect of
270 ophiolite conductivity and thickness. The ophiolite is thus simply a sink for heat energy and
271 not a source as in the previous described case. In the autochthon, as in the model described
272 above, temperatures steadily increase at a rate governed by the overlying ophiolite
273 conductivity and thickness and basal heat flow and underlying conductivity model. There is
274 also a lateral temperature gradient in the “ophiolite delta” case as the transient has had more
275 time to develop in the rear of the advancing slab, but there is not in the pelagic rain approach.
276 I notice that in Figs 7 d and e the ophiolite a temperature structure is left white. Why?

277 We left it white to focus the reader on the analysed passive margin units below. As correctly
278 stated above, we are not modelling the thermal evolution within the ophiolite (which is not
279 necessary as the rocks of the carbonate platform show no thermal overprinting from above;
280 a potential heating by a potentially warm ophiolite would in a maximal case effect the units
281 of the sedimentary nappes only).

282 But I can see the temperature structure in the ophiolite in Fig 8 where it is indeed a transient
283 warming from an initial uniformly cold state which looks to be about 30 deg C. I conclude that
284 the ophiolite is modeled purely as a heat sink. I find it geologically difficult to understand how
285 the entire slab can have got this cold in the actual obduction process

286

287 The sensitivity analyses presented and the back-up data in supplementary information are all
288 variations of the sedimentation modeling approach. For me they don’t help address the actual
289 sensitivities unless and until there is some justification for the sedimentation approximation
290 being a good one. See above, we do not use a sedimentation approach.

291

292 The model output is tuned to an accepted, reasonable, simulation because it matches
293 observed temperatures and pressures.

294

295 I would like to see some justification for why the cold “sedimentation” approach, with
296 a completely different set of transients, should be expected to give meaningful results for an
297 initially hot (even if by the time of interest strongly-cooled and cooling) thrust slab. I would
298 also like to understand why, even if the temperature history is matched, the modelled
299 thickness that goes with those temperatures and hence the pressures, be a good match to
300 reality.

301 We have to keep in mind, that the manuscript focusses on the thermal evolution of the
302 passive margin and not the one of the sedimentary nappes or the ophiolite. Therefore, as

303 stated by the reviewer, the “emplacement” approach is useful. However, if future work aims
304 to focus on the ophiolite, a different modelling approach needs to be tested.
305 To avoid misunderstanding we changed the methods part and added: “Modelling ophiolite
306 obduction as rapid deposition accounts for burial related heat effects in the carbonate
307 platform underneath, but this approach does not allow temperature modelling within the
308 ophiolitic or sedimentary nappes.”and “ This is based on the assumption that a possible heat
309 source represented by the ophiolite itself is not affecting the temperature of the top of the
310 carbonate platform (see discussion).”
311 I apologise if I’ve completely misunderstood or otherwise missed the point here, but at the
312 least, I find the current text and explanation to be an inadequate description of the
313 modelling method and assumptions.

Tectono-thermal evolution of Oman's Mesozoic passive continental margin under the obducting Semail Ophiolite: a case study of Jebel Akhdar, Oman

Arne Grobe^{1,2}, Christoph von Hagke¹, Ralf Littke², István Dunkl³, Franziska Wübbeler¹, Philippe Muchez⁴, Janos L. Urai^{1,5}

¹Structural Geology, Tectonics, and Geomechanics, EMR Group, RWTH Aachen University, Germany

²Geology and Geochemistry of Petroleum and Coal, EMR Group, RWTH Aachen University, Germany

³Sedimentology & Environmental Geology, Geoscience Center Georg-August-Universität Göttingen, Germany

⁴Geodynamics and Geofluids Research Group, Department of Earth and Environmental Sciences, KU Leuven, Belgium

⁵Department of Applied Geoscience, German University of Technology in Oman GUtech, Muscat, Oman.

Correspondence to: Arne Grobe, arne.grobe@rwth-aachen.de, ORCID: 0000-0001-6471-0624

Keywords: basin modeling, passive margin, obduction, burial, Raman spectroscopy, thermochronology, thermal maturity

Abstract. We present a study of the pressure and temperature evolution in the passive continental margin under the Oman Ophiolite, using numerical basin models calibrated with thermal maturity data, fluid inclusion thermometry and low-temperature thermochronometry, [and building on the results of recent work on the tectonic evolution](#). Because the Oman Mountains experienced only weak post-obduction overprint, they offer a unique natural laboratory for this study.

Thermal maturity data from the Adam Foothills constrain burial in the basin in front of the advancing nappes [has been to](#) at least 4 km. Peak temperature evolution in the carbonate platform under the ophiolite depends [on the burial depth and](#) only weakly on the temperature of the overriding nappes which have cooled during transport from the oceanic subduction zone to emplacement. Fluid-inclusion thermometry yields pressure-corrected homogenization temperatures of 225 to 266 °C for veins formed during progressive burial, 296-364 °C for veins related to peak burial and 184 to 213 °C for veins associated with late-stage strike-slip faulting. In contrast, the overlying Hawasina nappes have not been heated above 130-170 °C, as witnessed by only partial resetting of the zircon (U-Th)/He thermochronometer.

In combination with independently determined temperatures from solid bitumen reflectance, we infer that the fluid inclusions of peak-burial-related veins formed at minimum pressures of 225-285 MPa. This implies that the rocks of the future Jebel Akhdar Dome were buried under 8-10 km of ophiolite on top of 2 km of sedimentary nappes, in agreement with thermal maturity data of solid bitumen reflectance and Raman spectroscopy.

Rapid burial of the passive margin under the ophiolite results in sub-lithostatic pore pressures, as indicated by veins formed in dilatant fractures in the carbonates. We infer that overpressure is induced by rapid burial under the ophiolite. Tilting of the carbonate platform in combination with overpressure in the passive margin caused fluid migration towards the south in front of the advancing nappes.

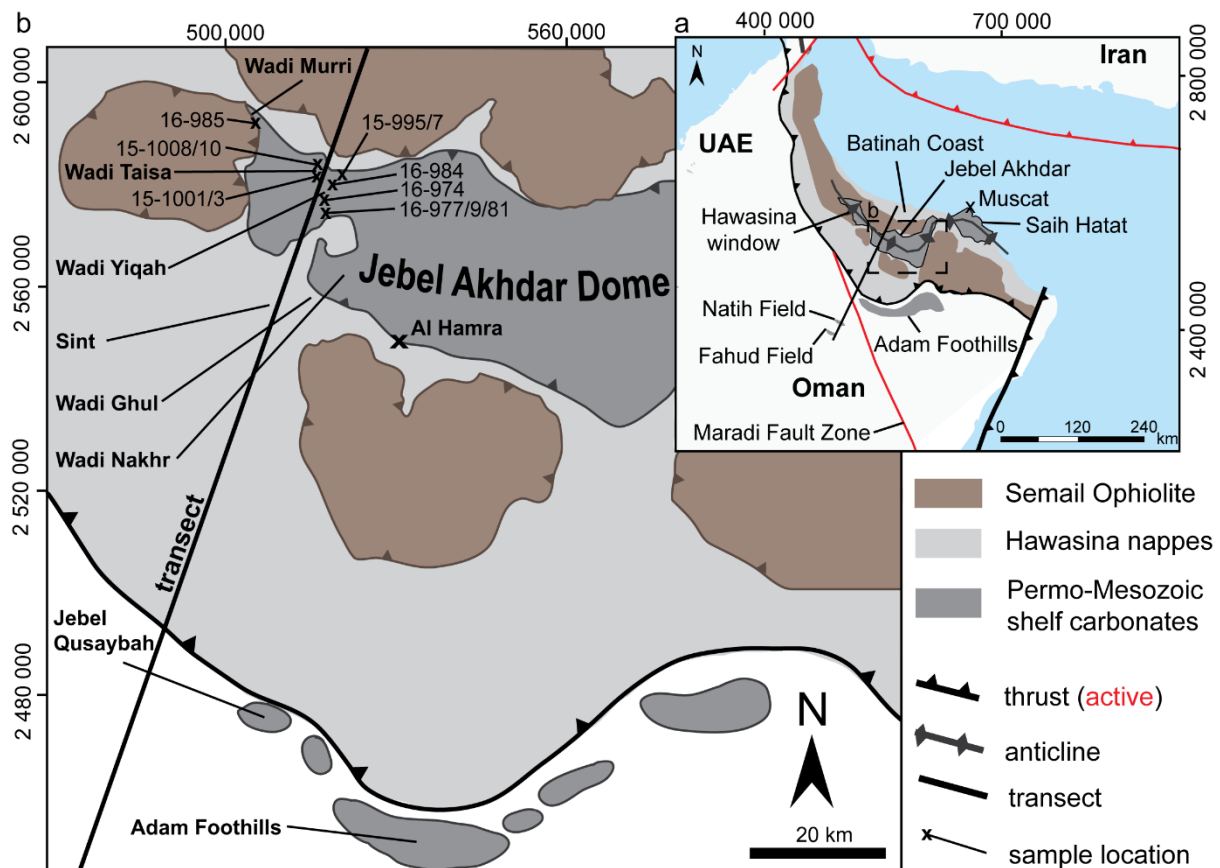
Exhumation of the Jebel Akhdar as indicated by our zircon (U-Th)/He data and [integrated-in agreement](#) with existing [structural interpretations and data work on the tectonic evolution](#), started as early as the late Cretaceous to early Cenozoic, linked with extension above a major listric shear zone with top-to-NNE shear sense. In a second

42 exhumation phase the carbonate platform and obducted nappes of the Jebel Akhdar Dome cooled together below
43 c. 170 °C between 50 and 40 Ma, before the final stage of anticline formation.

44 **1. Introduction**

45 The Permian-Mesozoic platform sediments of north Oman (Figure 1; e.g. Beurrier et al., 1986; Glennie et al.,
46 1974; Lippard et al., 1982) with hydrocarbon accumulations in the southern foreland of the Jebel Akhdar Dome
47 (Figures 1 and 2) are overlain by the Semail ophiolite nappe complex, the largest and best-preserved ophiolite on
48 Earth. Limited tectonic extension after obduction followed by uplift, folding and deep erosion and the present-
49 day arid climate formed exceptional exposures in three tectonic windows and in the foreland fold-and-thrust belt
50 of the Oman Mountains (Figure 1). The structural [and tectonic](#) evolution of the Oman Mountains has been one
51 main focus of our group in the last 15 years (e.g. Arndt et al., 2014; Gomez-Rivas et al., 2014; Grobe et al., 2016,
52 2018; Hilgers et al., 2006; Holland et al., 2009a; Virgo et al., 2013a, 2013b) and was investigated in many other
53 studies focusing on tectonic history (Breton et al., 2004; Cooper et al., 2014; Glennie et al., 1973, 1974; Grobe et
54 al., 2018; Loosveld et al., 1996; Searle, 2007), stratigraphic sequences (Van Buchem et al., 2002; Grelaud et al.,
55 2006; Homewood et al., 2008), geodynamic modelling (Duretz et al., 2015), hydrocarbon source rocks (Van
56 Buchem et al., 1996; Philip et al., 1995; Scott, 1990) and reservoir rocks (Arndt et al., 2014; De Keijzer et al.,
57 2007; Koehrer et al., 2011; Virgo et al., 2013a). Less well known is the temperature and pressure evolution of the
58 subophiolite passive margin units and the subsequent cooling history of the Jebel Akhdar (Aldega et al., 2017;
59 Grobe et al., 2018; Hansman et al., 2017; Poupeau et al., 1998; Saddiqi et al., 2006). This information is vital for
60 our understanding of the time-temperature history [of overthrust margins](#) and would allow to further constrain
61 obduction dynamics and forebulge migration. Combining peak temperature evolution with cooling ages links the
62 burial history with phases of orogeny.

63



64

65

66

67

68

69

70

Figure 1: a) Tectonic setting of the Oman Mountains. Shaded in Dark gray are the three tectonic windows of Hawasina, Jebel Akhdar and Saih Hatat as well as the Adam Foothills. Brown areas show the exposed Semail Ophiolite, black lines denote the obduction fronts of Semail and Masirah ophiolites, red lines denote lithosphere-scale, active structures/faults. The modeled transect (black line) crosscuts the Jebel Akhdar window and continues to the Natih and Fahud oil fields in the southwestern mountain foreland. b) Geologic map of the Jebel Akhdar window with the location of the modeled transect (solid black line) and the locations of thermal maturity data (x).

71

72

73

74

75

76

77

78

79

80

81

82

83

84

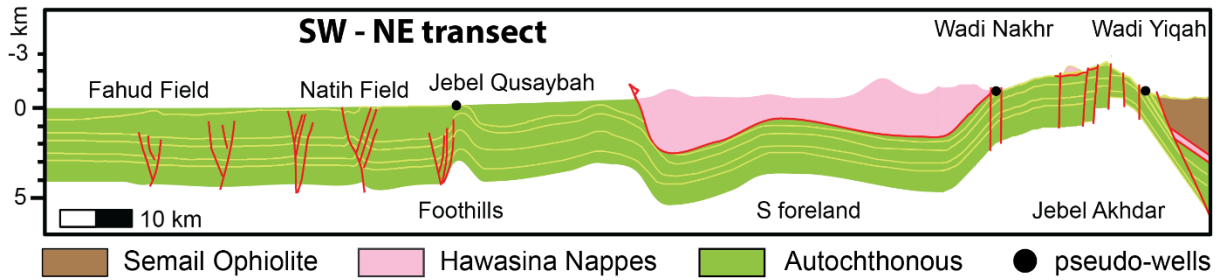
85

86

In other orogens, peak temperatures related to nappe emplacement were reconstructed by analyzing thermal maturity of finely dispersed organic material (e.g. Teichmüller and Teichmüller, 1986; Zagros: Mashhadi et al., 2015; Holy Cross Mountain: Schito et al., 2017; Eastern Alps: Lünsdorf et al., 2012; Southern Alps: Rantitsch and Rainer, 2003; Apennines: Reutter et al., 1988). However, the number of studies of thermal and pressure effects on overthrust sedimentary basins is limited and modeling approaches to reconstruct such large scale overthrusts are increasing but still few (e.g. Aldega et al., 2018; Deville and Sassi, 2006; Ferreiro Mählmann, 2001; Jirman et al., 2018; Oxburgh and Turcotte, 1974; Roure et al., 2010; Schito et al., 2018; Wygrala, 1989). In these studies, a main difficulty is to differentiate between temperature history of overthrusting and overprinting by later phases of orogeny. In the Oman Mountains, peak temperatures reached by obduction have not been overprinted. The whole Permian-Mesozoic sequence of the carbonate platform below the ophiolite is well exposed, providing outcrop to study the pressure and temperature history of this rapidly buried passive-margin sequence.

In this paper we present new thermal maturity, thermochronology and fluid inclusion data, and integrate them in a numerical basin model of the pressure-temperature evolution along a transect extending from the undeformed passive margin sequence in the south to the Batinah coast in the north (Figure 2). This helps to constrain temperature and pressure conditions of maximum burial, and the time of dome formation and exhumation linked to the structural and tectonic evolution of the area (Grobe et al., 2018). Our results for the Oman Mountains can

87 be used to understand more deformed orogens, shed light to fluid migration in the early stages of orogeny and on
 88 exhumation related to orogenic collapse.
 89



90
 91 **Figure 2: Structural transect used for modeling the Jebel Akhdar Dome and its southern foreland (Al-Lazki et al.,**
 92 **2002; Filbrandt et al., 2006; Searle, 2007; Warburton et al., 1990). Highlighted are the locations of the pseudo-wells**
 93 **(white-black circles) in Wadi Nakhr, Wadi Yiqah and at Jebel Qusaybah, Adam Foothills, which were used for model**
 94 **calibration.**

95 2. Geological setting

96 2.1. Tectonic setting

97 Along the northeastern coast of Arabia, the NW-SE oriented Oman Mountains form a more than 400 km long
 98 anticlinal orogen (Figure 1). The mountain belt consists of allochthonous sedimentary and ophiolitic nappes thrust
 99 onto a Permian-Mesozoic passive continental margin (Breton et al., 2004; Glennie et al., 1973; Loosveld et al.,
 100 1996; Searle and Cox, 2002).

101 This continental margin was formed during opening of the Neotethyan ocean (Loosveld et al., 1996) and the
 102 formation of the Permian-Mesozoic Hawasina Basin (Béchenec et al., 1988; Bernoulli et al., 1990). The initiation
 103 of subsea thrusting of the future Semail Ophiolite onto the Arabian Plate at 97-92 Ma, is recorded by U-Pb
 104 geochronology (Rioux et al., 2013, 2016; Warren et al., 2005) and $^{40}\text{Ar}/^{39}\text{Ar}$ dating of the metamorphic sole
 105 (Hacker et al., 1996). The advancing ophiolite caused a flexural forebulge that moved southwestwards through
 106 the passive margin during the Upper Cretaceous (Robertson, 1987). Forebulge migration induced up to 1100 m
 107 of uplift of the Permian-Mesozoic Arabian Platform and erosion of the Cretaceous platform sediments (Searle,
 108 2007), causing the Wasia-Aruma Break (Robertson, 1987).

109 During this convergence, parts of the Hawasina ocean sediments and volcanic units became detached and accreted
 110 in front of and beneath the ophiolite nappe (Béchenec et al., 1988, 1990; Glennie et al., 1974; Searle et al., 2003;
 111 Warburton et al., 1990). Palinspastic reconstructions of the Hawasina Nappes locate the position of the initial
 112 ophiolite thrusting 300-400 km offshore the Arabian coast (Béchenec et al., 1988; Glennie et al., 1974).

113 In the carbonate platform, burial under the advancing nappes led to generation of overpressure cells and formation
 114 of three crack-seal calcite vein generations (Gomez-Rivas et al., 2014; Grobe et al., 2018; Hilgers et al., 2006;
 115 Holland et al., 2009a; Virgo, 2015). The highest grades of metamorphism is recorded by eclogites exposed in As
 116 Sifah (Figure 1a), at c. 79 Ma (Warren et al., 2003).

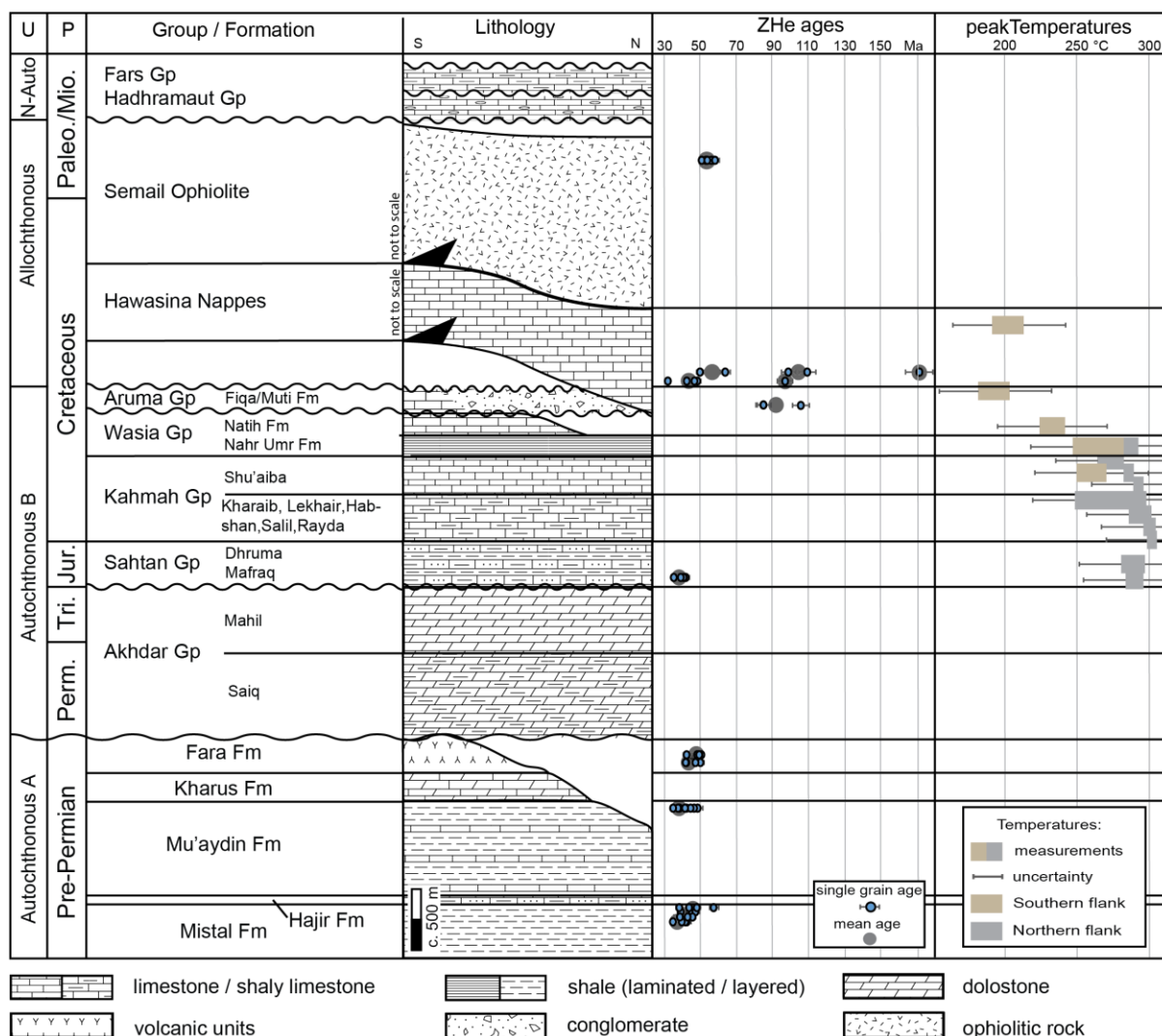
117 The sedimentary record in the Batinah coast and the foreland, as well as laterite formation on top of the ophiolite
 118 suggest subaerial exposure and a slow-down or stopped obduction before lower marine conditions were restored
 119 in the Maastrichtian (Coleman, 1981; Forbes et al., 2010; Nolan et al., 1990). This slowdown might relate to the
 120 formation of the Makran subduction zone (Agard et al., 2005; Grobe et al., 2018; Hassanzadeh and Wernicke,
 121 2016; Jacobs et al., 2015; Mouthereau, 2011) preserving the early stage of the obduction orogen in Oman.

122 In the Jebel Akhdar, post-obduction extension took place along ductile top-to-NNE shear zones, at 64 ± 4 Ma
123 (Grobe et al., 2018; Hansman et al., 2018), followed by NW-SE striking normal fault systems (Al-Wardi and
124 Butler, 2007; Fournier et al., 2006; Grobe et al., 2018; Hanna, 1990; Hilgers et al., 2006; Holland et al., 2009a,
125 2009b; Loosveld et al., 1996; Mattern and Scharf, 2018; Virgo, 2015).

126 Renewed Arabia-Eurasia convergence during the Cenozoic formed the three dome structures. Timing of formation
127 and exhumation of the Jebel Akhdar Dome is still debated. Stratigraphic arguments for a late Cretaceous doming
128 are Maastrichtian rocks unconformably deposited on Hawasina (Bernoulli et al., 1990; Fournier et al., 2006;
129 Hanna, 1990; Nolan et al., 1990), while inclined Miocene strata at the northern fringes of the dome points to a
130 Miocene doming (Glennie et al., 1973). Consequently, some models suggest a two-phased exhumation in
131 Cretaceous and Miocene (Grobe et al., 2018; Searle, 1985, 2007), in agreement with thermochronological
132 constraints and an interpreted two-stage cooling with possible reheating in late Miocene (Poupeau et al., 1998;
133 Saddiqi et al., 2006). More recent studies, however, have shown that the data can also be explained by a cooling-
134 only scenario with exhumation in the Eocene (Hansman et al., 2017). This is in agreement with recent structural
135 observations suggesting early dome formation and later amplification of the structure (Grobe et al., 2018).

136 **2.2. Stratigraphic sequence**

137 Sediments in the Jebel Akhdar area consist of a pre-Permian sequence (Autochthonous A, Figure 3)
138 unconformably overlain by a Permian-Mesozoic sequence (Autochthonous B, Figure 3; Beurrier et al., 1986;
139 Breton et al., 2004; Glennie et al., 1974; Rabu et al., 1990). During the late Cretaceous, Hawasina nappes and the
140 Semail Ophiolite were emplaced onto the passive margin, and neo-autochthonous rocks of Cenozoic age were
141 deposited on top of the ophiolite after obduction (Béchenec et al., 1988; Forbes et al., 2010; Loosveld et al.,
142 1996).



143
144
145
146
147
148
149
150

151
152
153
154
155
156
157
158
159
160
161
162

Figure 3: Stratigraphy of the Jebel Akhdar area with its two passive margin sequences Autochthonous A and B overthrust by Hawasina and Semail Nappes and unconformably overlain by neo-autochthonous units. Thermal calibration data is shown: ZHe ages (Table 2) show two different grain age clusters. Peak burial temperatures from organic matter maturity (Table 1) outline the temperature increase with stratigraphic age. *Temperature data was supplemented by values from *Mozafari et al. (2015) and +Grobe et al. (2016).* (U = Unit, P =Period). Note that the Semail and Hawasina nappes are shown in their structural rather than stratigraphic positions; lithological data is compiled from Beurrier et al. (1986), Loosveld et al. (1996), Terken et al. (2001) and Forbes et al. (2010).

Autochthonous A deposits are exposed in the Jebel Akhdar window down to the Mistal Fm. (Beurrier et al., 1986). Black limestones of the Hajir Fm., mudstone rich carbonate beds of the Mu'aydin Fm. and lime- and dolostones of the Kharus Fm. conformably overlie the Mistal Fm. (Beurrier et al., 1986; Glennie et al., 1974). Platform break-up is recorded by laminated cherts and volcanoclastics of the Fara Fm. (Beurrier et al., 1986) followed by an unconformity representing a gap from Cambrian to Permian times (Loosveld et al., 1996). After establishment of the Neotethyan Ocean during the Permian, northern Oman returned to stable passive margin conditions and the carbonate platform of the Autochthonous B developed, with the Akhdar Group at its base (Koehrer et al., 2010; Pöppelreiter et al., 2011). This is unconformably overlain by limestones with clastic interlayers of the Jurassic Sahtan Group (Beurrier et al., 1986; Pratt et al., 1990). Limestones with marly, frequently organic-rich intercalations of the Cretaceous Kahmah (Habsi et al., 2014; Vahrenkamp, 2010) and Wasia groups (Grelaud et al., 2006; Homewood et al., 2008; Philip et al., 1995) form the youngest platform sediments (Robertson, 1987; Warburton et al., 1990).

163 The obduction-related moving forebulge and associated uplift ended passive margin deposition and eroded the
164 topmost Wasia Group (Natih Fm.) in the Jebel Akhdar (**Figure 3**), and deeper in the Saih Hatat region. Deposition
165 in the foredeep basins in front and behind the forebulge was dominated by the syn- and postorogenic,
166 conglomerate-rich sediments of the Muti Fm., Aruma Group (Beurrier et al., 1986; Robertson, 1987). Towards
167 the south, in the Adam Foothills, this laterally grades to calcareous foreland sediments of the Fiqa Fm. (Forbes et
168 al., 2010; Robertson, 1987; Warburton et al., 1990).
169 Hawasina sediments accreted in front and beneath the ophiolite represent marine slope and basin facies, time
170 equivalent to the Autochthonous B (Béchenec et al., 1990). They are defined as four age-equivalent groups
171 (Hamrat Duru, Al Aridh, Kawr and Umar) representing carbonate; turbidite deposits (Hamrat Duru Group),
172 radiolarian cherts and platform carbonates (Al Aridh Group), platform carbonates (Kawr Group) and interbedded
173 carbonates and volcanics (Umar Group). (Béchenec et al., 1990). After obduction of oceanic crust onto the
174 passive margin, neo-autochthonous evaporites and carbonates of the Paleocene to Eocene Hadhramaut Gp. and
175 bivalve-rich dolomites and limestones of the Oligo- to Pliocene Fars Group were deposited south of the mountains
176 (Béchenec et al., 1990; Forbes et al., 2010). Paleogeographic reconstructions show that the Oman Mountains had
177 high relief after obduction, followed by a low relief landscape until the early Eocene (Nolan et al., 1990). In the
178 middle Eocene marine transgression caused widespread deposition of limestones, as witnessed e.g. by the Seeb
179 and Ruwaydah Formations (Nolan et al., 1990). Post Eocene times show renewed relief development and
180 continued uplift until recent times (Glennie et al., 1974; Searle, 2007).

181 **2.3. Previous paleothermal data of the Autochthon**

182 Only limited paleo-temperature data are available from the carbonate platform (Fink et al., 2015; Grobe et al.,
183 2016; Holland et al., 2009a; Stenhouse, 2014). Peak-burial temperatures of 226-239 °C for the top of the platform
184 were measured using solid bitumen reflectance (also referred to as pyrobitumen reflectance) and Raman
185 spectroscopy of carbonaceous material (RSCM) in the Jebel Akhdar (Grobe et al., 2016). Results indicate peak-
186 burial temperatures of 266 to 300 °C (Grobe et al., 2016; Table 1). Temperature estimates based on RSCM and
187 solid bitumen reflectance (Grobe et al., 2016) yielded similar temperatures for the southern flank of 248-280 °C
188 for the Nahr Umr, 226-239 °C for the Natih B and 172-206 °C for the Muti, respectively (Table 1, Figure 3).
189 Vein crystallization temperatures of 166-205 °C at the top of the Natih A (near Al Hamra) were measured by
190 quartz-calcite thermometry in veins formed during ophiolite-induced burial (Gen. III of Grobe et al., 2018), and
191 approximately 255 °C for veins associated with a later normal fault network (Gen V of Grobe et al., 2018;
192 Stenhouse, 2014). Fluid inclusions (FI) of bedding parallel pinch-and-swell veins (top-to-NNE shear after peak
193 burial, Gen. IV of Grobe et al., 2018) show uncorrected minimum trapping temperatures of 134-221 °C in the
194 lower beds of the Sahtan Group at Wadi Nakhr (Holland et al., 2009a). Reflectance measurements of solid-
195 bitumen-containing veins in the Wadi Ghul (Gen I of Grobe et al., 2018), which are interpreted to be associated
196 with fluid mobilization during forebulge migration, showed maximum temperatures of 230 °C (Fink et al., 2015).
197 Vitrinite reflectance data of Mozafari et al. (2015) shows temperatures of c. 140 °C for the Natih B in the Jebel
198 Qusaybah, Adam Foothills, an area not overthrust by the ophiolite complex.

199 **2.4. Temperature evolution of the Semail Ophiolite nappe / Allochthon**

200 Initial intra-oceanic ophiolite thrusting and associated metamorphism at its sole took place at peak temperatures
201 of 840 ± 70 °C at 97-92 Ma measured at several locations in the Oman Mountains (Gnos and Peters, 1993; Hacker
202 and Mosenfelder, 1996; Rioux et al., 2013; Searle and Cox, 2002; Warren et al., 2003). At 90-85 Ma the base of
203 the ophiolite cooled to 350 ± 50 °C (white mica Ar/Ar dating, Gnos and Peters, 1993). At around 80 Ma the
204 deepest burial of the Oman margin beneath the ophiolite was reached (Hacker and Mosenfelder, 1996; Warren et
205 al., 2005) with temperatures in the metamorphic sole below 300 °C (Le Metour et al., 1990; Saddiqi et al., 2006).
206 A lithospheric scale thermo-mechanical model of the thrusting in northwestern Oman includes a thermal anomaly
207 c. 100 km northwest offshore the Arabian margin to initiate subsea thrusting (Duretz et al., 2015).

208 **2.5. Petroleum system elements**

209 Several petroleum systems developed in the carbonate platform of northern Oman with important source rock
210 horizons in the Natih Fm. (Members B and E). Both members contain Type I/II kerogen with total organic carbon
211 contents up to 15 % in the Natih B and up to 5 % in the Natih E, respectively (Terken, 1999). Source rock maturity
212 is restored based on biomarker analysis to c. 0.7 %VR within the Fahud reservoir and c. 0.9 %VR in the Natih
213 reservoir (Terken, 1999). In the southern mountain foreland Natih oil generation started in the middle Cretaceous
214 and continuous until present (Terken, 1999). Ophiolite obduction in the Jebel Akhdar area of northern Oman led
215 to over-mature Natih source rocks (Grobe et al., 2016). The Natih is classified as supercharged, laterally drained,
216 foreland petroleum system (Terken et al., 2001). However, the thermal impact of the moving forebulge and the
217 importance of tectonic processes for fluid migration below and in front of the obduction orogen are not clear. At
218 least three different generations of solid bitumen particles in veins and source rocks on the southern slope of the
219 Jebel Akhdar suggest pulses of hydrocarbon generation and migration in front of the Oman Mountains (Fink et
220 al., 2015; Grobe et al., 2016). In central Oman, Shu'aiba and Tuwaiq oils are produced out of Kahmah and Sahtan
221 Group reservoirs, sealed by argillaceous shales of the Nahr Umr Fm. (Terken et al., 2001). All these units are
222 well-exposed in the Oman Mountains.

223 **3. Methods**

224 **3.1. Raman spectroscopy of carbonaceous material**

225 To determine levels of thermal maturity, over 100 dark, unweathered and organic-rich samples were taken from
226 different stratigraphic units in the Jebel Akhdar (Sahtan Group, Kharaib Fm., Shu'aiba Fm., Nahr Umr Fm., Natih
227 Fm., Muti Fm., **Figure 3**). Based on total organic carbon (TOC) content as determined by Grobe et al. (2016), 13
228 samples were selected for thermal maturity analysis on surfaces cut perpendicular to bedding. Results were used
229 to calibrate peak-burial temperatures of the numerical basin models. The organic particles lack sufficient size or
230 surface quality for reflectance measurements and are therefore investigated by confocal Raman spectroscopy of
231 carbonaceous material. The technique measures vibrational energies of chemical bonds which change during
232 temperature induced reorganization of amorphous carbonaceous material (kerogen) to graphite (e.g. Aoya et al.,
233 2010; Beyssac et al., 2002; Kouketsu et al., 2014; Mair et al., 2018). Measurements were conducted at the
234 Geoscience Center, Göttingen, on a Horiba Jobin Yvon HR800 UV spectrometer attached to an Olympus BX-41
235 microscope and a 100× objective. A high-power diode laser with a wavelength of 488 nm and an output power of

236 50 mW was installed and a D1 filter avoided sample alteration by heating. Each spectral window (center at
237 1399.82 cm^{-1} , grid of 600 lines/mm) was measured 5 to 10 times for 2 to 10 seconds with a Peltier CCD detector
238 at activated intensity correction. For quality control, the 520.4 cm^{-1} line of a Si-wafer was measured every 30
239 minutes without observable drift of the measurements. To transform the measured data into VR_r values the scaled
240 total area (STA) approach of Lünsdorf (2016) was applied with the equation of Grobe et al. (2016):

$$241 \quad VR_r = -\frac{STA - 280.13}{24.71} \quad [\%]$$

242 Absolute errors of the applied calibration are in the order of $\pm 40\text{ }^\circ\text{C}$, based on comparing neighboring samples
243 (Grobe et al., 2016) we can resolve the relative differences down to $\pm 30\text{ }^\circ\text{C}$ which also represents the residual
244 error interpreted to relate to within-sample heterogeneity (Lünsdorf et al., 2017; Nibourel et al., 2018).

245 3.2. Fluid inclusion thermometry

246 Doubly-polished wafers (c. $200\text{ }\mu\text{m}$ thick) of four vein samples (FI-N1, -N2, -M1, -M2) have been prepared
247 according to the procedure described by Muchez et al. (1994). Fluid inclusion (FI) petrography and
248 microthermometry was performed to analyze the temperature-pressure conditions and fluid's salinity. FIs
249 represent paleofluids accidentally trapped in a crystalline or amorphous solid during crystallization, lithification
250 or both (Diamond, 2003). If unaffected by later changes, trapping pressure and temperature is given by the
251 homogenization temperature (Barker and Goldstein, 1990). Based on the time of trapping primary (mineral
252 growth), secondary (fracture-related) and pseudosecondary inclusions are distinguished (Barker and Goldstein,
253 1990; Diamond, 2003; Goldstein, 2001; Van Den Kerkhof and Hein, 2001):

254 Two calcite vein samples of the Natih Fm. (FI-N1 and 2, Locations **Figure 4**) represent conditions related to early
255 burial (FI-N2, structural generation I of Grobe et al., 2018), and burial beneath the ophiolite (FI-N1, structural
256 generation III of Grobe et al., 2018). Two quartz-rich calcite veins of the Muti Fm. (FI-M1 and 2, Locations **Figure**
257 **4**) are related to late, NE-SW striking strike slip faults (generation IX of Grobe et al., 2018). FI assemblages were
258 defined and fluid inclusions measured with a Linkam THMSG600 thermostage (accuracy $\pm 0.1\text{ }^\circ\text{C}$) attached to
259 an Olympus BX60 microscope at the KU Leuven, Belgium. Calibration was performed using CO_2 , $\text{H}_2\text{O-NaCl}$,
260 $\text{H}_2\text{O-KCl}$, and H_2O standards. Homogenization temperatures (T_h) were measured prior to temperatures of
261 complete freezing (T_f), first melt (T_{fm}), and complete melting of ice ($T_{m(ice)}$) to avoid stretching or leakage due to
262 the volume increase during ice formation. All measured temperatures were recorded during heating, except for
263 the freezing temperature (T_f). Pressure corrections of T_h were conducted with the program FLINCOR (Brown,
264 1989) for 280 and 340 MPa, assuming 8 to 10-km of ophiolite overburden (see model results, $\rho = \text{c. } 3070\text{ kg/m}^3$)
265 and 2-km of ~~sedimentary~~-Hawasina Nappes ($\rho = \text{c. } 2450\text{ kg/m}^3$), and for 45 MPa, assuming 2-km of sedimentary
266 overburden (Al-Lazki et al., 2002; Grobe et al., 2016). Fluid salinities were calculated from the $T_{m(ice)}$ values
267 considering a $\text{H}_2\text{O-NaCl}$ composition (Bodnar, 1993), which is based on the T_{fm} values.

268 3.3. Thermochronometry

269 Zircon (U-Th)/He (ZHe) dating allows to reconstruct the thermal history of the topmost few kilometers of the
270 Earth's crust. Helium retention in less metamict zircon crystals is sensitive in the temperature range between
271 c. 130 and $170\text{ }^\circ\text{C}$, i.e. the zircon partial retention zone (PRZ, Reiners, 2005). 11 rocks sampled above (Muti Fm.,
272 Matbat Fm. of the Hamrat Duru Group~~Hawasina~~ and Trondjemite of the Semail nappes), below (Mistal Fm.,
273 Muaydin Fm., Fara Fm.) and within (Sahtan Gp.) the carbonate platform were selected for ZHe dating. Zircon

274 crystals were released using high voltage pulse crushing (<http://www.selfrag.com>) and concentrated by standard
275 mineral separation processes (drying, dry sieving, magnetic and heavy liquid separation). Three to eight clear,
276 intact, euhedral single crystals were selected per sample and transferred into platinum micro-capsules. They were
277 degassed under high vacuum by heating with an infrared diode and extracted gas purified using a SAES Ti-Zr
278 getter at 450 °C. Helium was analyzed with a Hiden triple-filter quadrupole mass spectrometer. Degassed zircons
279 were subsequently dissolved in pressurized teflon bombs, spiked and U, Th and Sm measured with a Perkin Elmer
280 Elan DRC II ICP-MS equipped with an APEX micro flow nebulizer.

281 Time-temperature histories were reconstructed using the HeFTy 1.8.3 software package (Ketchum, 2005)
282 applying kinetic zircon properties of Guenther et al. (2013). For samples with reset zircons the only constraint
283 used was a minimum temperature above 200 °C between deposition and the calculated ZHe age. Thermal
284 modeling was conducted until 100 statistically good time-temperature paths were achieved (goodness of fit: 0.5,
285 value for acceptable fit: 0.05). In cases where this was not possible, at least 10,000 independent paths were
286 calculated.

287 3.4. Numerical basin modeling

288 Structural evolution was palinspastically reconstructed starting from the present-day profile using Move 2D
289 (2016.1, Midland Valley Exploration). Geometries and relative ages of the structures were supplemented with
290 subsurface data (Al-Lazki et al., 2002; Filbrandt et al., 2006; Searle et al., 2004; Warburton et al., 1990). The
291 reconstruction workflow is based on restoring the pre-deformation layer continuity as follows: (1) faulted layers
292 in the southern foreland were restored, (2) doming was retro-deformed by vertical simple shear, before (3) normal
293 faults in the Jebel Akhdar were restored. This sequence is based on our tectonic model (Grobe et al., 2018). The
294 resulting geometries were used as pre-thrusting input geometries for 2D PetroMod 2014.1 (Schlumberger) basin
295 modeling, enabling thermal maturity reconstruction for vitrinite reflectance values of 0.3 to 4.7 % by the use of
296 the EASY % Ro approach (Sweeney and Burnham, 1990). The numerical basin model is based on a conceptual
297 definition of events. Based on this sequence of events (sedimentation, erosion, hiatus) a forward, event-stepping
298 modeling was performed, starting with the deposition of the oldest layer. Subsequent deposition and burial is
299 leading to differential compaction of the single rock units. For each event lithologies and related petrophysical
300 rock properties were assigned (Figures S1, S2).

301 For our conceptual model the following sequence of events was implemented (Figure 3): (1) passive margin
302 carbonate sedimentation from Permian until late Cenomanian times (Forbes et al., 2010; Loosveld et al., 1996),
303 interrupted by a short erosional period at the Triassic-Jurassic boundary (Koehrer et al., 2010; Loosveld et al.,
304 1996), (2) a moving forebulge associated with a paleo-water depth increase in its foredeep and erosion of the top
305 of the carbonate platform in the north of the transect (Robertson, 1987), (3) the emplacement of allochthonous
306 sedimentary nappes and (4) subsequent, ~~stepwise~~-obduction, ~~i.e. stepwise, rapid sedimentation~~, of the ophiolite
307 with deepest burial reached at c. 79 Ma (Warren et al., 2005). Modelling ophiolite obduction as rapid emplacement
308 accounts for burial related heat effects in the carbonate platform underneath, but does not allow to fully restore
309 the temperatures modelling within the ophiolitic or sedimentary nappes. The area of the Adam Foothills,
310 represented in the transect by Jebel Qusaybah, is a relic of the moving forebulge not overthrust by allochthonous
311 units – this was used to calibrate burial depth of the foredeep at this point in the transect. The area to the south of
312 the Adam foothills is unaffected by foredeep sedimentation~~The south of the foothills is unaffected by foredeep~~

313 ~~and obduction~~, but also lacks thermal calibration data. Absolute ages, thicknesses, lithologies and related
314 petrophysical properties as well as source rock properties were associated according to results of our own field
315 mapping and the compiled data from Forbes et al. (2010; Figure S1).

316 Thermal boundary conditions of the model have been defined for each time step by the basal heat flow (HF) and
317 the sediment water interface temperature (SWIT), representing the upper thermal boundary (Figure S3). To
318 account for active margin tectonics and uplift and exhumation of the Jebel Akhdar, we assume an increase in basal
319 heat flow since the late Cretaceous. The resulting heat flow trend (Figure S3, Terken et al., 2001; Visser, 1991)
320 has been assigned to the entire transect and was tested in the sensitivity analysis. Paleo-surface temperatures were
321 estimated based on Oman's paleo-latitude (after Wygrala, 1989) corrected by the effect of the paleo-water depth
322 (PWD) derived from the facies record (Van Buchem et al., 2002; Immenhauser et al., 1999; Immenhauser and
323 Scott, 2002; Koehrer et al., 2010; Pratt et al., 1990; Robertson, 1987). This assumes that a possible heat source
324 from the ophiolite itself does not significantly affect the temperature evolution of the top of the carbonate platform
325 (see discussion).

326 This set-up has been iterated until modeling results fit the thermal calibration data (Table 1). From VR_r
327 calculations peak-burial temperatures were determined following the approach of Barker and Pawlewicz (1994).
328 For calibration of the numerical basin models, data was supplemented by thermal maturity and peak-burial
329 temperature data of 63 Natih B source rock samples, taken around the Jebel Akhdar Dome (Grobe et al., 2016),
330 and data from the Adam Foothills on Jebel Qusaybah (Mozafari et al., 2015).

331 Main modelling uncertainties derive from the uncertainty in thickness of paleo-overburden (Muti Fm., Ophiolite,
332 Hawasina Nappes) and uncertainty of paleo-basal heat flow. Present-day heat flow was calibrated by data and
333 borehole temperatures of Visser (1991) and Rolandone et al. (2013) and peak-burial temperatures determined by
334 Raman spectroscopy and solid bitumen reflectance data (Table 1). From surface samples and their position in the
335 stratigraphic column various pseudo-wells were created (e.g. Nöth et al., 2001) and used as control points for the
336 2D model (Figure 2). The model was used for sensitivity analyses of different input parameters.

337 4. Results and Interpretation

338 4.1. Thermal maturity and host rock burial temperatures

339 New Raman spectroscopy data of the northern flank are shown in Table 1 and give scaled total areas of 78-172.
340 This correspond to peak temperatures of 270-300 °C in the Shu'aiba Fm., 268-305 °C in the Kahmah Group, 283-
341 286 °C in the Sahtan Group, 270-288 °C in the Nahr Umr Fm. and c. 266 °C at the base of the Natih Fm. Based
342 on the calculation to VR_r and temperature an absolute error of ± 30 °C has to be considered for the single values.

343 Thermal maturity data of the Natih Fm. show solid bitumen reflectances of 2.95-3.72 % for the southern flank of
344 the Jebel Akhdar (Fink et al, 2015, Grobe et al., 2016), 3.32 % BR for the northern flank (Grobe et al., 2016) and
345 a single measurement of 1.1 % VR exists for the Jebel Qusaybah (Mozafari et al., 2015).

346 Calculated peak temperatures for the autochthonous Cretaceous deposits in the Jebel Akhdar range between 225
347 and 305 °C (± 30 °C, error of the calibration), two Jurassic samples 283 and 286 °C (± 30 °C). Temperatures are
348 generally higher on the northern flank (grey boxes, Figure 3) of the Jebel Akhdar and slightly increase with
349 stratigraphy in the autochthonous. Samples of the Muti Fm. (178-208 ± 30 °C) and the Hawasina nappes (193-
350 213± 30 °C) show lower temperatures compared to the autochthonous. A single sample from the Jebel Qusaybah

351 reflects peak temperatures of c. 140 °C (Table 1) in an area that was not overthrust by nappes but buried in the
 352 related moving forebulge.

353 **Table 1: Thermal maturity data and calculated peak temperatures of northern Oman (new data highlighted by bold**
 354 **sample name). Temperatures from Raman spectroscopy of carbonaceous material are calculated based on the STA**
 355 **approach of Lünsdorf (2016) and the equation of Grobe et. al (2016). M/P indicate if measurement was conducted on**
 356 **solid bitumen particles (P) or organic rich matrix (M). Errors shown relate to the measurements, calculation errors**
 357 **are in the order of +/-30 °C. Data in brackets is interpreted to be too low (Nahr Umr) or too high (Natih Vein, Fink et**
 358 **al. 2015).**

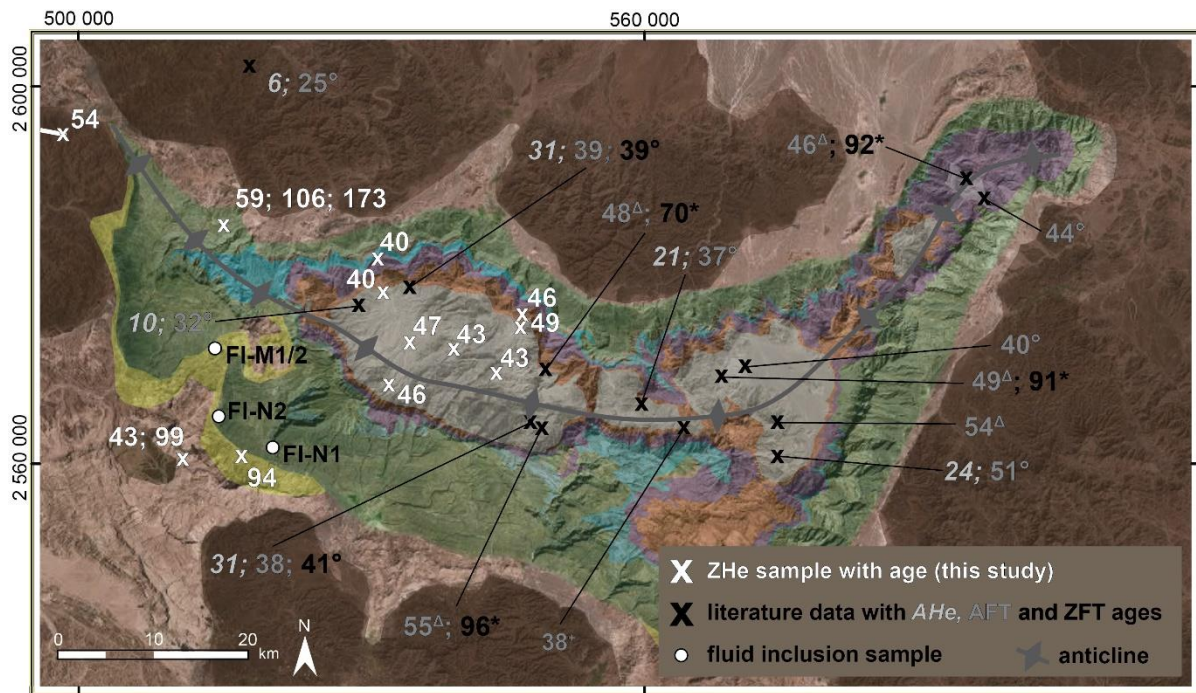
sample No.		location (UTM 40Q)					No. of measurements	mean D_STA	calculated VR, [%]	temperature range
15_995	northern flank	Wadi Yiqah	516683	2582911	Sahtan Gp.	M	14	113 +/- 14	6,52	286 +/- 6 °C
15_997		Wadi Yiqah	517815	2583645	Shu'aiba Fm.	M	10	115 +/- 5	6,69	289 +/- 3 °C
15_1001		Wadi Taisa	516538	2584640	Kahmah Gp.	M	1	78	8,19	305 °C
15_1003		Wadi Taisa	516538	2584640	Kahmah Gp.	M	8	96 +/- 9	7,44	297 +/- 4 °C
15_1008		Wadi Taisa	516562	2584727	Kahmah Gp. (top)	M	8	113 +/- 15	6,78	290 +/- 7 °C
15_1010		Wadi Taisa	516693	2584882	Shu'aiba Fm.	M	13	98 +/- 11	7,28	295 +/- 5 °C
15_1010		Wadi Taisa	516693	2584882	Shu'aiba Fm.	P	4	149 +/- 15	5,31	270 +/- 9 °C
16_974		Tr- Jur fault	515839	2582229	base Sahtan Gp.	P	6	125 +/- 17	6,29	283 +/- 9 °C
16_977		Kharb Plateau	520420	2577490	base Natih Fm.	M	10	156 +/- 9	5,04	266 +/- 6 °C
16_979		Kharb Plateau	519305	2577363	top Nahr Umr Fm.	M	2	117 +/- 4	6,60	288 +/- 2 °C
16_981		Kharb Plateau	519933	2577201	top Nahr Umr Fm.	M	1	149	5,30	270 °C
16_984		Wadi Taisa	518069	2583462	Kahmah Gp.	M	3	172 +/- 26	5,29	268 +/- 22 °C
16_985		Wadi Murri	505508	2592709	Shu'aiba Fm.	M	2	90 +/- 4	7,69	300 +/- 2 °C
Grobe et al. (2016)_SV10		southern flank	Wadi Nakhr	521260	2560364	Natih	P	6	-	2,83
Grobe et al. (2016)_AG22	Wadi Nakhr		521255	2560362	Natih	M	4	-	3,72	225-260 °C
Grobe et al. (2016)_AG01	Wadi Nakhr		520375	2562026	Shu'aiba (Kh 3)	M	4	-	4,49	251-269 °C
Grobe et al. (2016)_AG11	Sint		505627	2564136	Hawasina	P	5	-	2,45	193-213 °C
Grobe et al. (2016)_AG25	Balcony Walk Nakhr		520913	2565658	Nahr Umr	M	4	-	4,23	226-267 °C
Grobe et al. (2016)_AG26_1	Balcony Walk Nakhr		521052	2565560	Nahr Umr	P	2	-	(2.58)	(211-213 °C)
Grobe et al. (2016)_AG26_3	Balcony Walk Nakhr		521052	2565560	Nahr Umr	M	2	-	4,96	275-280 °C
Grobe et al. (2016)_AG27	Balcony Walk Nakhr		520879	2565342	Nahr Umr	M	3	-	4,61	248-266 °C
Grobe et al. (2016)_AG30	Balcony Walk Nakhr		520756	2565030	Nahr Umr	M	3	-	4,25	248-257 °C
Grobe et al. (2016)_AG37	Jebel Shams		514821	2568047	Muti	P	3	-	2,16	191-208 °C
Grobe et al. (2016)_AG38	Jebel Shams		514930	2567334	Muti	P	2	-	1,99	172-206 °C
reference			location (UTM 40Q)					No. of measured particles	measured BR, [%]	calculated / measured VR, [%]
Grobe et al. (2016)	N south. fl.	Wadi Nakhr area	521216	2560308	Natih B	BR _v	253	3.08-3.59	3.08-3.59	226-239 °C
Fink et al. (2015)		Wadi Nakhr area	518550	2561000	Natih B	BR _v	200	3.10-3.14	3.06-3.09	225-227 °C
Fink et al. (2015)		Wadi Nakhr area	514800	2565950	Natih A Vein	BR _v	c. 250	3.40-3.76	(3.31-3.61)	(232-239 °C)
Grobe et al. (2016)		Al Hamra area	531024	2557020	Natih B	BR _v	20	2.95-3.34	2.95-3.34	223-233 °C
Grobe et al. (2016)	N	Wadi Sahtan	531010	2585640	Natih B	BR _v	6	3,32	3,32	232 °C
Mozafari et al. (2015)		Jebel Qusaybah	507930	2491600	Natih B	VR _v	20	-	1,1	c. 140 °C

359

360 4.2. Thermochronology

361 Results of the ZHe dating are shown in Figures 3 and 4; time-temperature paths modeled with HeFTy are included
 362 in the electronic supplement (Figures S4 and S5). Samples from the carbonate platform (stratigraphically older
 363 than Muti Fm.) have been entirely reset after deposition, as witnessed by Neogene apparent ages. Similarly,
 364 cooling ages from the center of the Jebel Akhdar Dome fall in the range of 48.7 ± 1.8 to 39.8 ± 3.0 Ma (Table 2,
 365 **Figure 4**). Sample T4, collected in the Muti Fm., yields an apparent mean age of 93.8 ± 6.9 Ma and samples T5

366 and T7 of the Hawasina Nappes collected at the northern and the southern slope of the dome, show two grain age
 367 clusters of $43.0 \pm 3.7 / 99.2 \pm 8.5$ Ma, and $58.9 \pm 7.0 / 106.0 \pm 5.2$ Ma, respectively. In sample T5, an additional
 368 single grain age of 172.9 ± 14.9 Ma was obtained.
 369



370
 371 **Figure 4: Map view of ZHe ages (in Ma).** Data outlines a general cooling between 58.9 ± 7.0 and 39.8 ± 3.0 Ma. Some
 372 samples outside of the dome show two age clusters, with an additional age of c. 100 Ma. Additional temperature data
 373 refers to zircon fission track ages of (*) Saddiqi et al. (2006), Apatite fission track ages of (Δ) Poupeau et al. (1998) and
 374 (+) Mount et al. (1998), and AHe, AFT and ZFT ages of (+, grey) Hansmann et al. (2017). Moreover, the locations of
 375 samples used for fluid inclusion measurements are shown. Colors in the background depict geological units (brown:
 376 ophiolite, pink: Hawasina units, light green: Muti Fm., dark green: Wasia and Kahmah Gp., blue: Sahtan Gp., purple:
 377 Mahil Fm, orange: Saiq Fm, grey: pre-Permian, shaded DEM from Esri, Digital Globe, swisstopo, and the GIS user
 378 Community).

379 **Table 2: Results of zircon (U-Th)/He dating.**

sample aliquot	lithology / location Easting Northing		He		²³⁸ U			²³² Th			Th/U ratio	Sm			ejection correct. (Ft)	uncorr. He age [Ma]	FT corrected				mean age [Ma]
			vol. [ncc]	1 σ [%]	mass [ng]	1 σ [%]	conc. [ppm]	mass [ng]	1 σ [%]	conc. [ppm]		mass [ng]	1 σ [%]	conc. [ppm]			correct. (Ft)	He age [Ma]	He age [Ma]	2 σ [%]	
T1-21	sandstone		5.31	0.83	1.04	1.81	212.00	0.38	2.41	77.66	0.37	0.03	10.43	6.44	0.754	38.90	51.60	8.20	4.20	48.70 +/- 1.80	
T1-22	547533	2574875	6.05	0.84	1.31	1.81	323.34	0.33	2.41	80.49	0.25	0.01	21.24	2.97	0.737	36.10	49.10	8.70	4.30		
T1-23	Fara Fm.	Autochthon A	3.45	0.87	0.84	1.81	212.21	0.30	2.41	74.73	0.35	0.02	14.08	3.83	0.719	31.30	43.60	9.20	4.00		
T1-24			3.15	0.86	0.64	1.82	178.10	0.34	2.41	95.86	0.54	0.01	15.61	4.16	0.72	36.30	50.50	9.10	4.60		
T2-21	tuffite		9.23	0.83	2.04	1.81	352.85	1.03	2.41	178.16	0.50	0.04	9.53	7.26	0.778	33.40	42.90	7.60	3.20	46.10 +/- 2.00	
T2-22	547533	2574875	8.58	0.83	1.99	1.81	376.54	0.88	2.41	166.07	0.44	0.07	7.63	14.20	0.757	32.30	42.70	8.10	3.50		
T2-23	Fara Fm.	Autochthon A	12.48	0.83	2.32	1.81	377.81	1.01	2.41	163.95	0.43	0.03	11.07	5.44	0.789	40.20	51.00	7.30	3.70		
T2-24			6.16	0.83	1.26	1.81	186.92	0.52	2.41	76.65	0.41	0.03	10.98	4.83	0.768	36.80	48.00	7.80	3.80		
T3-21	sandstone		3.69	0.86	1.04	1.81	361.71	0.41	2.41	142.73	0.39	0.02	15.90	6.29	0.689	26.90	39.10	10.00	3.90	42.60 +/- 1.70	
T3-22	544722	2570255	2.82	0.88	0.63	1.82	254.57	0.22	2.42	87.47	0.34	0.02	12.85	9.07	0.694	34.20	49.40	9.90	4.90		
T3-23	Muaydin Fm.	Autochthon A	1.54	0.90	0.35	1.85	116.01	0.23	2.42	75.70	0.65	0.02	17.64	5.19	0.67	31.80	47.50	10.50	5.00		
T3-24			4.71	0.84	1.20	1.81	309.13	0.70	2.41	180.18	0.58	0.05	9.18	12.12	0.74	28.50	38.50	8.60	3.30		
T3-25			8.91	0.83	1.95	1.81	262.57	1.30	2.41	175.08	0.67	0.07	9.00	9.29	0.761	32.60	42.90	8.00	3.40		
T3-26			9.80	0.83	2.52	1.81	283.31	1.13	2.41	127.16	0.45	0.06	7.80	6.56	0.816	29.00	35.60	6.60	2.30		
T3-27			11.83	0.83	2.41	1.81	219.27	1.23	2.41	111.66	0.51	0.11	7.31	10.01	0.794	36.10	45.50	7.10	3.20		
T3-28			8.41	0.83	1.85	1.81	224.86	1.04	2.41	125.92	0.56	0.07	9.09	8.40	0.784	33.10	42.20	7.40	3.10		
T4-21	conglomerate		18.23	0.83	1.79	1.81	380.98	0.44	2.41	93.57	0.25	0.02	13.79	3.77	0.736	79.30	107.60	8.70	9.40	93.80 +/- 6.90	
T4-22	517510	2560808	10.68	0.83	1.36	1.81	392.55	0.35	2.41	100.65	0.26	0.02	15.99	5.30	0.703	61.20	86.90	9.60	8.40		
T4-23	Muti Fm.	Autochthon B	5.24	0.85	0.56	1.82	137.78	0.48	2.41	118.23	0.86	0.04	8.48	11.06	0.738	64.20	86.90	8.60	7.50		
T5-21	turbiditic sandstone		34.15	0.82	3.38	1.81	502.17	0.79	2.41	117.95	0.23	0.10	7.97	14.16	0.781	78.70	100.80	7.50	7.60	106.00 +/- 5.20	
T5-22	512934	2561691	13.52	0.83	1.28	1.81	333.42	0.27	2.41	69.42	0.21	0.02	16.57	4.11	0.744	82.70	111.20	8.50	9.50		
T5-23	Matbat Fm.	Hawasina N.	8.95	0.83	1.30	1.81	254.43	0.78	2.41	153.35	0.60	0.01	16.47	2.78	0.754	49.70	65.90	8.20	5.40		
T5-24			9.21	0.84	1.75	1.81	416.93	0.69	2.41	163.29	0.39	0.04	9.44	9.25	0.766	39.80	51.90	7.90	4.10		
T5-25			37.88	0.80	51.13	2.33	1.81	561.72	0.37	2.41	90.14	0.16	0.02	11.59	0.741	0.741	128.10	172.90	8.60		14.90
T6-21	granodiorite		6.55	0.83	1.00	1.81	241.80	1.28	2.41	311.91	1.29	0.29	5.62	69.36	0.747	41.60	55.60	8.30	4.60	53.70 +/- 1.20	
T6-22	478301	2592360	6.39	0.85	0.97	1.81	288.96	1.32	2.41	394.16	1.36	0.28	5.31	84.38	0.719	41.10	57.20	9.10	5.20		
T6-23	Trondjemite	Semail Ophio.	7.07	0.83	1.06	1.81	314.75	1.79	2.41	528.55	1.68	0.19	5.49	57.19	0.751	39.20	52.30	8.20	4.30		
T6-24			12.11	0.84	1.79	1.81	347.26	3.35	2.41	649.55	1.87	0.31	5.55	61.00	0.769	38.60	50.20	7.70	3.80		
T6-25			6.78	0.84	1.08	1.81	273.36	1.46	2.41	368.85	1.35	0.27	5.75	68.70	0.738	39.10	53.00	8.60	4.50		
T7-21	quartzite		14.91	0.84	1.56	1.81	427.30	0.43	2.41	118.20	0.28	0.05	9.26	12.45	0.744	73.80	99.20	8.50	8.50	99.20	
T7-22	514817	2586049	4.14	0.87	1.35	1.81	428.75	0.38	2.41	119.50	0.28	0.02	12.47	7.90	0.729	23.70	32.50	8.90	2.90		
T7-23	Matbat Fm.	Hawasina N.	6.37	0.85	1.33	1.81	274.36	0.30	2.41	62.67	0.23	0.03	10.62	6.71	0.769	37.50	48.80	7.90	3.80		
T7-24			9.66	0.81	12.43	2.13	1.81	539.06	0.15	2.45	38.38	0.07	0.01	17.24	0.777	36.90	47.50	7.70	3.70		
T7-25			4.03	0.83	5.46	0.94	1.81	232.12	0.47	2.41	115.05	0.50	0.02	12.63	0.738	31.70	43.00	8.60	3.70		
T8-21	tuffitic sandstone		4.60	0.86	1.34	1.81	450.89	1.11	2.41	374.66	0.83	0.16	5.81	53.52	0.759	23.70	31.20	8.00	2.50	39.80 +/- 3.00	
T8-22	532600	2578681	2.92	0.85	0.56	1.82	147.09	0.86	2.41	226.75	1.54	0.28	5.14	73.06	0.715	31.40	44.00	9.20	4.00		
T8-23	Mistal Fm.	Autochthon A	2.21	0.89	0.46	1.83	168.48	0.57	2.41	208.48	1.24	0.05	8.65	16.66	0.716	30.90	43.20	9.20	4.00		
T8-24			3.46	0.85	0.85	1.81	212.57	0.41	2.41	103.10	0.49	0.01	14.27	3.65	0.74	30.30	41.00	8.60	3.50		
T9-21	quartzite		2.90	0.86	0.61	1.82	238.35	0.50	2.41	198.12	0.83	0.01	16.09	5.23	0.705	33.10	46.90	9.50	4.50	45.50 +/- 2.40	
T9-22	532595	2568258	0.72	0.98	0.18	1.94	109.52	0.13	2.43	76.58	0.70	0.05	10.52	29.38	0.674	27.50	40.80	10.50	4.30		
T9-23	Mistal Fm.	Autochthon A	2.04	0.89	0.41	1.84	147.39	0.28	2.41	101.51	0.69	0.01	18.70	3.60	0.718	35.10	48.80	9.20	4.50		
T10-21	sandstone		5.09	0.85	0.93	1.81	213.39	0.95	2.41	217.83	1.02	0.02	13.41	4.93	0.754	36.40	48.20	8.10	3.90	46.90 +/- 4.10	
T10-22	534779	2572636	6.71	0.83	1.37	1.81	267.61	1.24	2.41	241.07	0.90	0.04	9.18	8.32	0.763	33.30	43.70	7.90	3.40		
T10-23	Mistal Fm.	Autochthon A	8.97	0.83	2.25	1.81	568.33	1.79	2.41	452.52	0.80	0.04	8.74	10.22	0.723	27.70	38.40	9.00	3.50		
T10-24			2.26	0.88	0.35	1.85	118.10	0.39	2.41	131.18	1.11	0.02	14.08	5.39	0.727	41.80	57.50	8.90	5.10		
T11-21	quartzite		4.70	0.84	1.01	1.81	188.02	0.57	2.41	106.02	0.56	0.01	19.39	2.18	0.746	34.00	45.60	8.40	3.80	42.50 +/- 2.00	
T11-22	540394	2572230	1.55	0.90	0.39	1.84	109.55	0.33	2.41	93.99	0.86	0.01	20.85	2.31	0.706	27.30	38.80	17.60	6.80		
T11-23	Mistal Fm.	Autochthon A	1.50	0.94	0.37	1.84	110.19	0.19	2.42	56.69	0.51	0.01	17.25	3.39	0.693	29.90	43.20	9.90	4.30		
T12-21	sandstone		5.35	0.85	1.21	1.81	355.93	1.09	2.41	320.43	0.90	0.02	16.47	5.58	0.706	30.10	42.70	9.50	4.00	40.10 +/- 1.50	
T12-22	531776	2582871	4.28	0.86	1.12	1.81	286.68	0.16	2.42	40.59	0.14	0.01	27.93	1.79	0.736	30.70	41.70	8.80	3.70		
T12-23	Sahtan Gp.	Autochthon B	3.80	0.86	1.06	1.81	349.54	0.14	2.43	44.41	0.13	0.01	22.03	2.70	0.719	28.70	39.90	9.20	3.70		
T12-24			1.51	0.89	0.38	1.84	92.50	0.32	2.41	76.60	0.83	0.01	15.61	3.53	0.758	27.30	36.10	8.10	2.90		

381 These ages indicate a large-scale cooling signal that affects the entire Jebel Akhdar area; the ZHe age pattern and
382 1D thermal models indicate a phase of rapid cooling below 170 °C in the early Cenozoic (58.9 ± 7.0 and
383 39.8 ± 3.0 Ma). The range of modeled cooling paths outline maximum cooling rates of 2-8 °C/Myr. This is
384 followed by slower cooling until the present day.

385 Data from the Muti Fm. and the Hawasina units differ partly from this trend: the apparent ZHe ages of clasts in
386 the Muti sample T4 (mean: 93.8 ± 6.9 Ma) is as old as its respective stratigraphic age (Robertson, 1987). Even
387 though all ages reproduce within error, this indicates partial reset of the ZHe system, as post-depositional reheating
388 above closure temperature would result in younger ages. Samples of the lower Hawasina Nappes contain two
389 grain age clusters. Older ages coincide with higher uranium concentrations suggesting that only the younger ages
390 represent thermally reset zircons. We note that the older ZHe ages of 110-95 Ma coincide with timing of forebulge
391 migration through the area, as independently determined in the stratigraphic record by the Wasia-Aruma Break
392 (Figure 3). This may be either pure coincidence, due to partial resetting of an older grain age population, or may
393 be a grain age population with higher closure temperature witnessing exhumation. We discuss reasons for different
394 resetting temperatures below. However, partial reset of ZHe ages suggests that the Hawasina samples have not
395 experienced temperatures exceeding the partial retention zone (PRZ) of 130-170 °C.

396 A sample from an intrusive body of the Semail Ophiolite yields ZHe ages of 53.7 ± 1.2 Ma (T6) with a modeled
397 cooling path gradually decreasing into the PRZ until c. 55 Ma. This time interval of passing the PRZ is comparable
398 to the Hawasina nappe samples beneath the ophiolite but occurs slightly earlier than cooling of the Autochthonous.
399 Nevertheless, Semail Ophiolite, Hawasina Nappes and the autochthonous margin sequence were affected by the
400 same cooling event that was possibly initiated by exhumation of the Jebel Akhdar Dome.

401 4.3. Fluid inclusions

402 The Muti veins' samples FI-M1 and M2 of the southern Jebel Akhdar show evidence of crack and seal processes
403 (youngest parts in the center of the vein, Ma-2010-11b and 14a of Arndt 2015) with blocky quartz grains that
404 contain two kinds of roundish primary FIs with sizes of 3-20 μm . They are mainly aligned along dark zones and
405 are interpreted as growth zones or form bright clusters in the central part of the crystals. A third set of fluid
406 inclusions (FIs) appears in large, grain-crosscutting trails interpreted to be of secondary origin. Calcite crystals
407 within the Natih veins contain bright FIs with sizes of 2-20 μm and are edgy, often rectangular or trapezoidal in
408 shape. Identified primary FIs are aligned parallel to crystal growth zones.

409 All measured FIs are two-phase, liquid-vapor inclusions with ice as last phase to melt. The Muti samples show
410 $T_{\text{fm(ice)}}$ between -5.1 ± 0.5 and -4.6 ± 0.3 °C and $T_{\text{m(ice)}}$ at -2.2 ± 0.2 to -1.9 ± 0.1 °C, the Natih sample T_{fm} of -
411 18.4 ± 1.9 to -20.2 ± 2.1 °C and $T_{\text{m(ice)}}$ of -7.1 ± 0.3 to -8.9 ± 1.8 °C (Table 3). First melting temperatures of all
412 inclusions correspond to an H₂O-NaCl system and complete melting temperatures of ice indicate salinities similar
413 to seawater (3.0 ± 0.5 to 3.5 ± 0.3 wt.-% NaCl eq., Muti Fm., Figure S6) or three times higher (10.3 ± 0.3 to
414 12.5 ± 2.0 wt.-% NaCl eq., Natih Fm., Figure S6).

415 **Table 3: Results of FI microthermometry. Identified FI types, their measured homogenization temperatures and results**
416 **of the pressure correction for 280 and 340 MPa accounting for 8 and 10 km of ophiolite with partly serpentinized**
417 **mantle sequence and 2 km of sedimentary-Hawasina nappes, and for 45 MPa accounting for 2 km of sedimentary**
418 **overburden for samples unaffected by ophiolite obduction. First melting (T_{fm}) and final melting of ice ($T_{\text{m(ice)}}$)**
419 **temperatures and salinities are given. Data by Holland et al. (2009) are added for comparison and we likewise corrected**
420 **their homogenization temperatures. (* further heating was avoided to prevent fluid inclusion damage)**

sample No.	vein orient., location and host mineral	FI kind	No. of FIA	T _h [°C]	pressure corrected T [°C] for 45 MPa		T _m [°C]	T _{m,ice} [°C]	salinity [wt.-% NaCl]
FI-M1	NE-SW striking	primary	21	166 +/- 7	189 +/- 7		-4.7 +/- 0.2	-2.2 +/- 0.2	3.5 +/- 0.3
	strike-slip vein (IX), Muti Fm.	primary	22	189 +/- 3	213 +/- 3		-4.6 +/- 0.3	-2.0 +/- 0.3	3.2 +/- 0.4
	Gorge area, quartz	secondary	18	> 200*	> 224		-4.6 +/- 0.2	-2.0 +/- 0	3.2 +/- 0
					pressure corrected T [°C] for 45 MPa				
FI-M2	NE-SW striking	primary	24	161 +/- 3	184 +/- 3		-5.1 +/- 0.5	-1.9 +/- 0.1	3.0 +/- 0.2
	strike-slip vein (IX), Muti Fm.	secondary	12	116 +/- 12	138 +/- 12		-	-	-
	Gorge area, quartz	secondary	24	150 +/- 2	172 +/- 2		-	-	-
					for 280 MPa	for 340 MPa			
FI-N1	Natih Fm., NW-SE	primary	14	90 +/- 5	235 +/- 5	266 +/- 5	-18.4 +/- 1.9	-7.1 +/- 0.3	10.3 +/- 0.3
	burial vein (III), Wadi Nakhr, calcite	primary	26	(114 +/- 7)	(264 +/- 7)	(297 +/- 7)	-20.2 +/- 2.1	-8.9 +/- 1.8	12.5 +/- 2.0
FI-N2	Natih Fm., early E-W vein (I)	primary	10	80 +/- 4	225 +/- 4	256 +/- 4	-	-	-
	Al Raheba, calcite								
					for 280 MPa	for 340 MPa			
Holland et al. (2009)	Sahtan Gp., bedding parallel shear vein, top-to-NE (IV), Wadi Nakhr, quartz	primary and pseudosec.	n.a.	134-141	296-303	357-364	from -19	-3.7 to -2.3	3.8 to 6.0

421

422

423

424

425

426

427

428

429

430

431

432

433

434

435

436

437

438

439

440

441

442

Primary inclusions in quartz crystals from the Muti Fm. show minimum trapping temperatures of 161 ± 3 to 166 ± 7 °C (Table 3, FI-M2 and middle of FI-M1) with a second primary population of 189 ± 3 °C (sides of vein FI-M1). T_h of secondary inclusions in FI-M1 are above 200 °C. In sample FI-M2, two generations of secondary inclusions were observed, both reflecting lower T_h than the primary inclusions. No hints of necking down, leakage or stretching were observed at the measured inclusions and over 90 % of the measured FIs in one assemblage are in the range of 10-15 °C representing a good quality of the measurements (Goldstein, 2001).

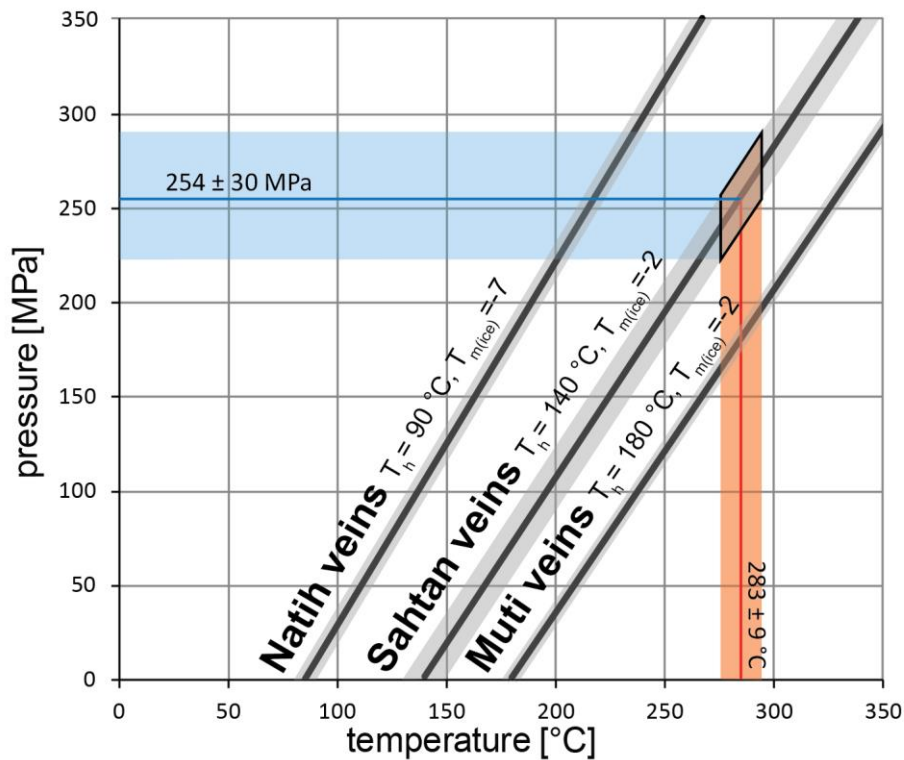
Samples FI-N1 and N2 of the Natih Fm. in the southern Jebel Akhdar (**Figure 4**) contain primary inclusions hosted by calcite crystals giving T_h of 80 ± 4 , 90 ± 5 and 114 ± 7 °C (Table 3). The latter population is often characterized by elongated, possibly stretched FI, and is not considered for further interpretations. Assuming vein formation during burial (Grobe et al., 2018; Hilgers et al., 2006; Holland et al., 2009a; Virgo, 2015) under 8 to 10 km of ophiolite including partially serpentized peridotite and 2 km of Hawasina Nappes, results were pressure corrected for 280 and 340 MPa leading to corrected homogenization temperatures of 235 ± 5 and 266 ± 5 °C (FI-N1), and 225 ± 4 and 256 ± 4 °C (FI-N2, Table 3). Signs of strong deformation such as twinning or cleavage were not observed in the measured inclusions; secondary inclusions were present but not measured.

These temperatures represent minimum trapping conditions of a paleo-fluid and do not necessarily represent burial temperatures of the host rock. It should be noted that the analyzed Natih veins formed bedding confined (Grobe et al., 2018; Holland et al., 2009a; Virgo, 2015) and show host rock buffered carbonate isotope signatures (Arndt et al., 2014; Hilgers et al., 2006). This corroborates the idea that analyzed veins were in thermal equilibrium with their host rocks.

FI microthermometry of late strike-slip veins in the Muti Fm. are interpreted to have formed after dome formation (Grobe et al., 2018; Virgo, 2015) at an assumed minimum depth of 2 km (preserved allochthonous thickness). A

443 pressure correction for the related 45 MPa corresponds to minimum fluid trapping temperatures of 184 ± 3 °C
 444 (FI-M2) and 213 ± 3 °C (FI-M1) with a later phase of primary inclusions outlining 189 ± 7 °C and even cooler
 445 secondary inclusions of 138 ± 12 to 172 ± 2 °C (FI-M1 and M2, Table 3). These cooler fluid temperatures can be
 446 explained by further exhumation of the Jebel Akhdar and, hence, cooling of the fluids' reservoir during crack-seal
 447 vein formation. Isotope studies on the vein calcite do not support an open system with fluid exchange (Stenhouse,
 448 2014; Virgo and Arndt, 2010), hence, we interpret the formation of strike-slip related veins as having formed
 449 during exhumation following peak burial.

450 Based on the assumption that fluid and host rock were in thermal equilibrium, we can use maturity data in
 451 combination with fluid inclusion data to estimate the pressure at vein formation. Peak temperatures of the Sahtan
 452 Group revealed by RSCM reached 283 ± 9 to 286 ± 6 °C (Table 1, **Figure 5** red line) and enable to solve the
 453 pressure-temperature couples of FIs measured in Sahtan veins formed at deepest burial by Holland et al. (2009,
 454 black line). This results in minimum trapping pressures of 254 ± 30 MPa at times of vein formation (**Figure 5** blue
 455 line), which correspond to times close to or at deepest burial of the carbonate platform.



456
 457 **Figure 5: Fluid inclusion isochores (solid black lines) of analyzed fluid inclusion populations with corresponding std.**
 458 **deviations (shaded areas, for Sahtan Group data of Holland et al., 2009, conservatively ± 10 °C are assumed). To**
 459 **estimate the pressure conditions during vein formation, calculated temperatures from thermal maturity data are added**
 460 **for the Sahtan Group (red line with error) and result in minimum trapping pressures of 254 ± 30 MPa during peak**
 461 **burial (blue line with error).**

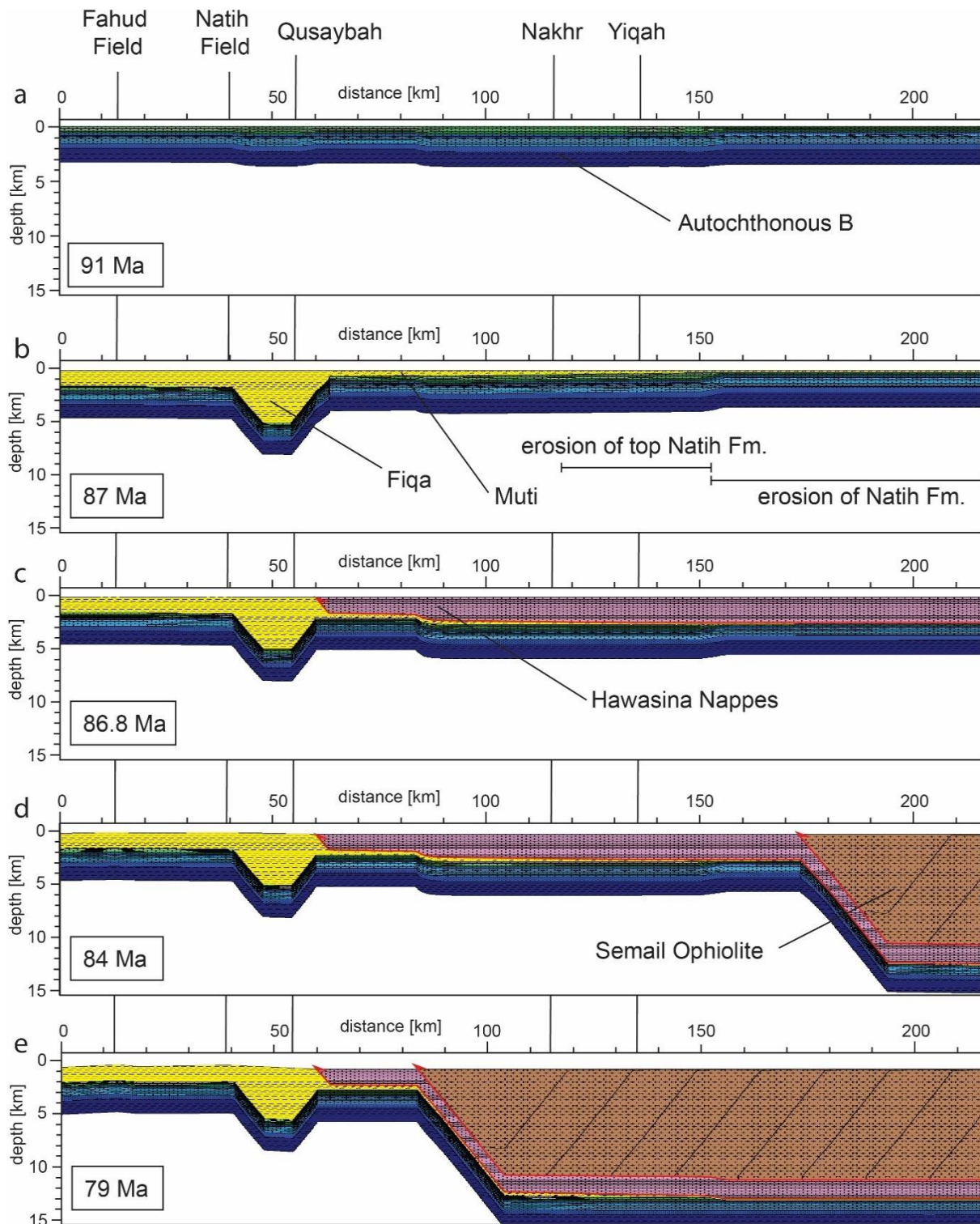
462 **4.4. Basin modeling**

463 Numerical basin modeling integrates all data and tests the individual interpretations in the thermal and
 464 geodynamic framework. Deepest burial was constrained with thermal maturity data and exhumation with
 465 thermochronological data. In the following we present our best fit model, considering a mixed ophiolite lithology

466 (Searle and Cox, 2002) consisting of strongly serpentized peridotites. Then, the sensitivity of important results
467 to changes of relevant input parameters are discussed.

468 Modeled evolution of the transect over time is given in Figures 6 and 7, showing (a) final deposition of the
469 Autochthonous B, (b) erosion of the Natih Fm. in the North by a moving foredeep (no erosion in S, full erosion
470 in N), (c) emplacement of 1400 m of Hawasina Nappes, and d-e) ophiolite obduction reconstructed by rapid,
471 stepwise sedimentation. After maximum burial beneath the ophiolite complex at c. 80 Ma (Warren et al., 2005)
472 exhumation is assumed to start slightly prior to 55 Ma (Saddiqi et al., 2006) with a rapid phase of cooling below
473 c. 200 °C at 55 Ma leading to lower temperatures in the Jebel Akhdar region. 1D burial plots of two pseudo-wells
474 created out of point data in Wadi Nakhr and Wadi Yiqah are shown in Figure 8.

475



476

477

478

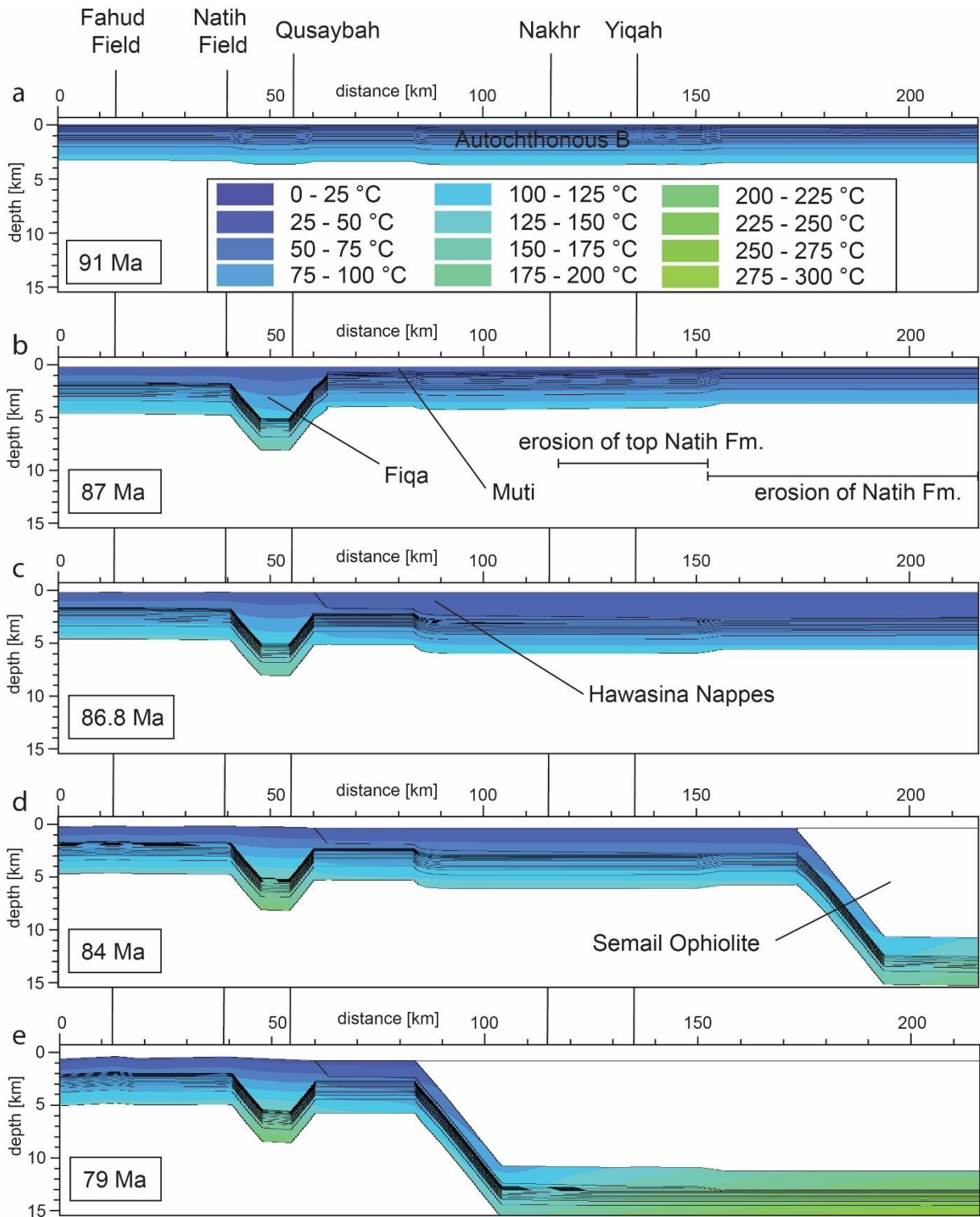
479

480

481

482

Figure 6: Modeling results: Transect evolution from sedimentation of the Autochthonous B at stable passive margin conditions (a), to moving foredeep that finally filled with Fiqa sediments (b, peak burial as calibrated by thermal maturity data), Hawasina Nappe (c) and ophiolite emplacement (d) leading to deepest burial (e). Highlighted with vertical lines in the background are the locations of present-day oil fields and sampled valley locations. Please note the unrealistically flat topography which is a result of the modelling set-up.

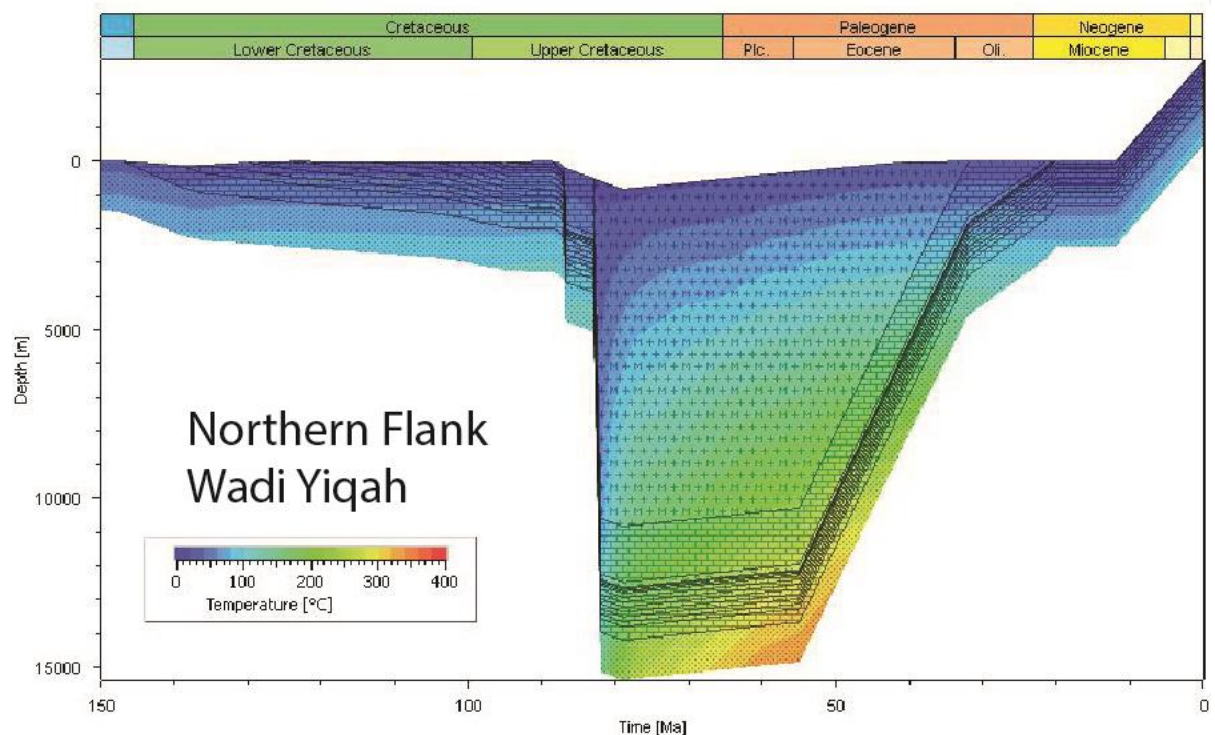
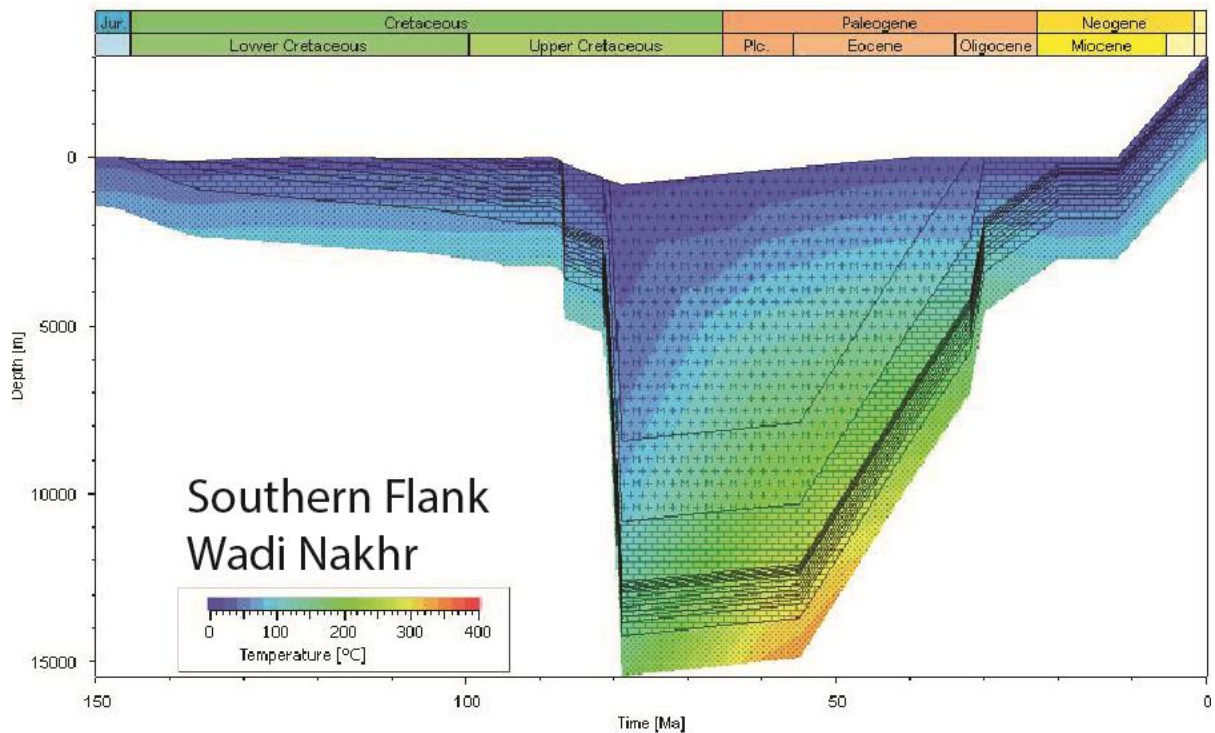


483

484

485

Figure 7: Modeling results: Temperature distribution and temporal evolution along the transect of Figure 6. Highlighted with vertical lines in the background are the locations of present-day oil fields and sampled valley locations.



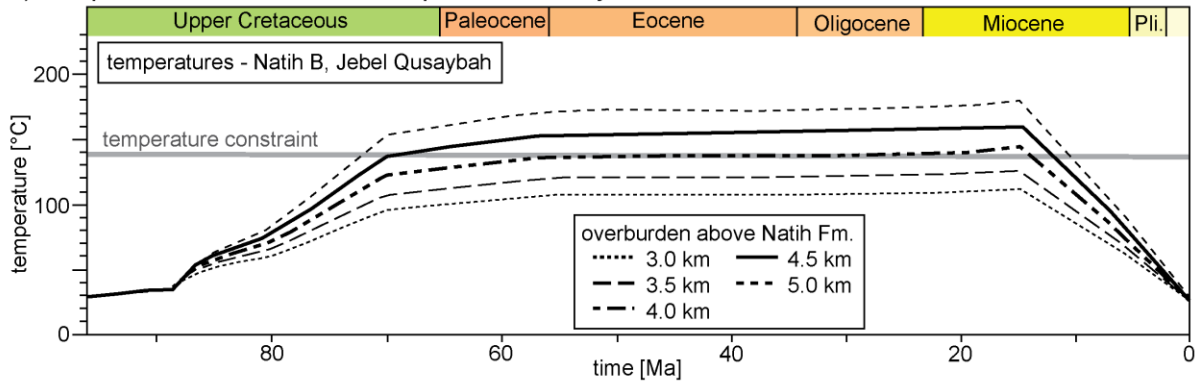
486

487 **Figure 8 Modeling results: Two representative burial plots for two pseudo-wells created near the entrances of Wadi**
 488 **Nakhr and Yiqah (Figures 1, 6 and 7) show two phases of rapid burial related to Hawasina and Semail Nappe**
 489 **emplacement and c. 88 Ma and ophiolite emplacement at c. 78 Ma. Burial in the North (Wadi Yiqah) starts c. 2 Myr**
 490 **earlier due to ophiolite obduction taking place from N to S.**

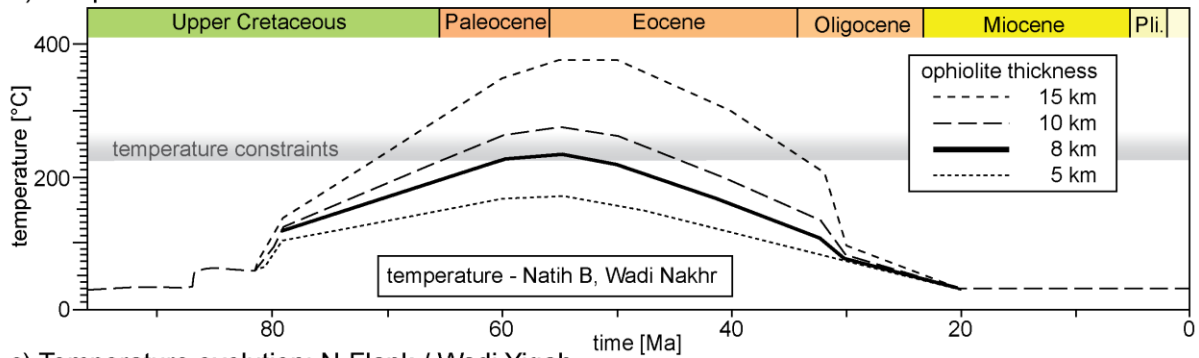
491 As a model set up only presents one possible solution out of several, sensitivity analyses with varying paleo-
 492 overburden thicknesses (Figures 9 and 10), changing degree of serpentinization of the ophiolite and varying basal
 493 heat flow during deepest burial (**Figure 11**) are presented and discussed below.

494 Thermal maturity data of the Natih B at Jebel Qusaybah (1.1 % VR_r), Adam Foothills, require peak temperatures
 495 of c. 140 °C (Table 1). Sensitivity analyses of the overburden above the Natih Fm. show that at least maximum
 496 4 km to 4.5 km of sedimentary overburden (Figures 9a and 10a) is needed to match the calibration data (Figures
 497 9a and 10a).
 498

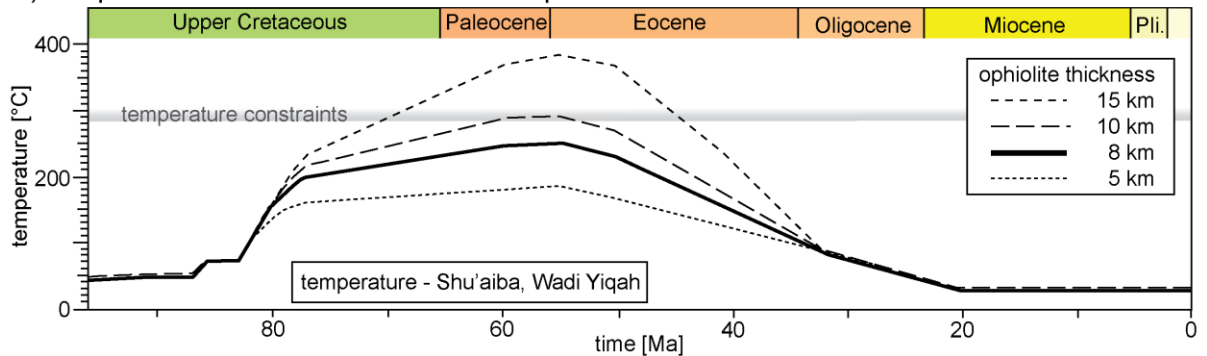
a) Temperature evolution: Foredeep / Jebel Qusaybah



b) Temperature evolution: S-Flank / Wadi Nakhr



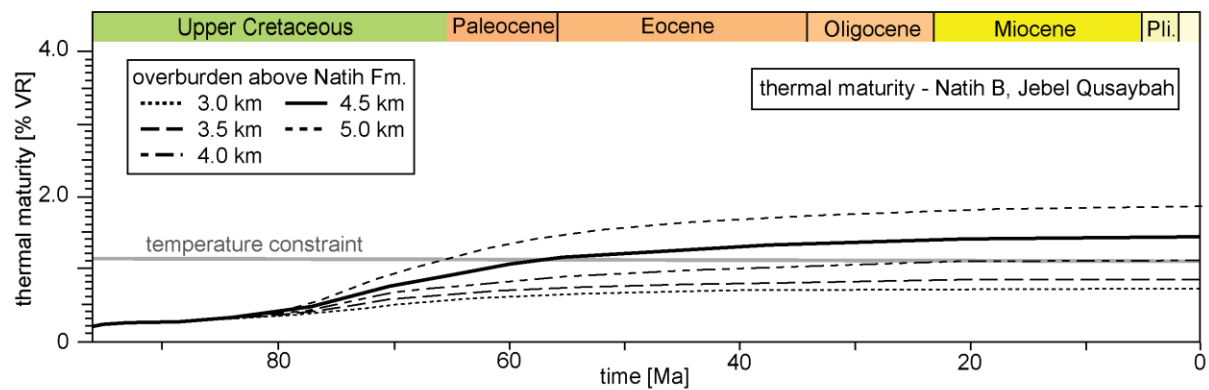
c) Temperature evolution: N-Flank / Wadi Yiqah



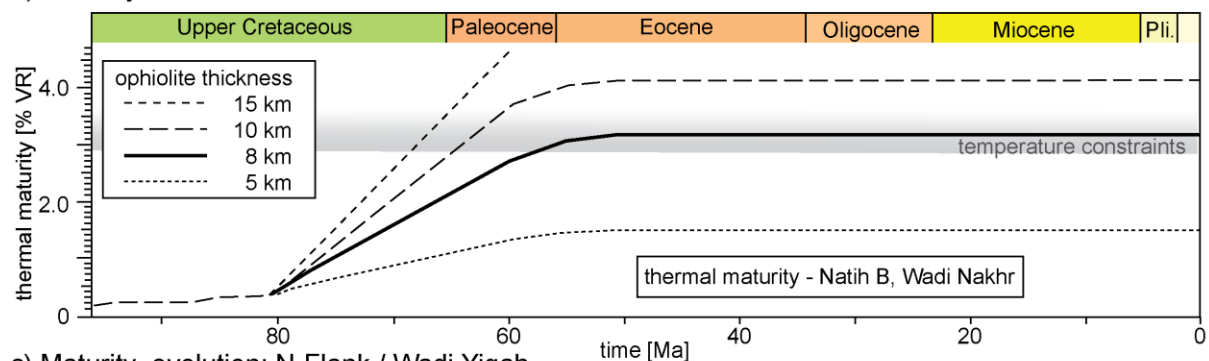
499

500 **Figure 9: Sensitivity analysis of paleo-overburden and its influences on temperature in comparison to calculated peak**
 501 **temperatures (gray area) for pseudo-wells at Jebel Qusaybah (a), Wadi Nakhr (b) and Wadi Yiqah (c).**

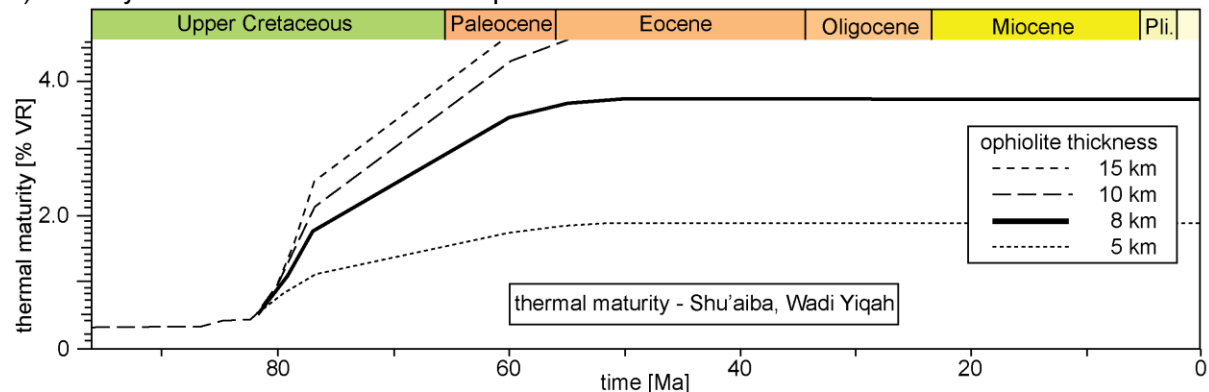
a) Maturity calibration: Foredeep / Jebel Qusaybah



b) Maturity calibration: S-Flank / Wadi Nakhr



c) Maturity evolution: N-Flank / Wadi Yiqah



502

503 **Figure 10: Sensitivity analysis of paleo-overburden and its influences on thermal maturity in comparison to calibration**
 504 **data (gray area). Data is used to calibrate burial depth of the foredeep at the Jebel Qusaybah (a) and the paleo-ophiolite**
 505 **thickness at the southern flank of the Mountains at Nakhr (b). Its northern counterpart at Yiqah (c) is in agreement**
 506 **with the temperature data of Figure 9, however to mature to be reconstructed by standard maturity modelling**
 507 **(Sweeney and Burnham, 1990).**

508

509

510

511

512

513

514

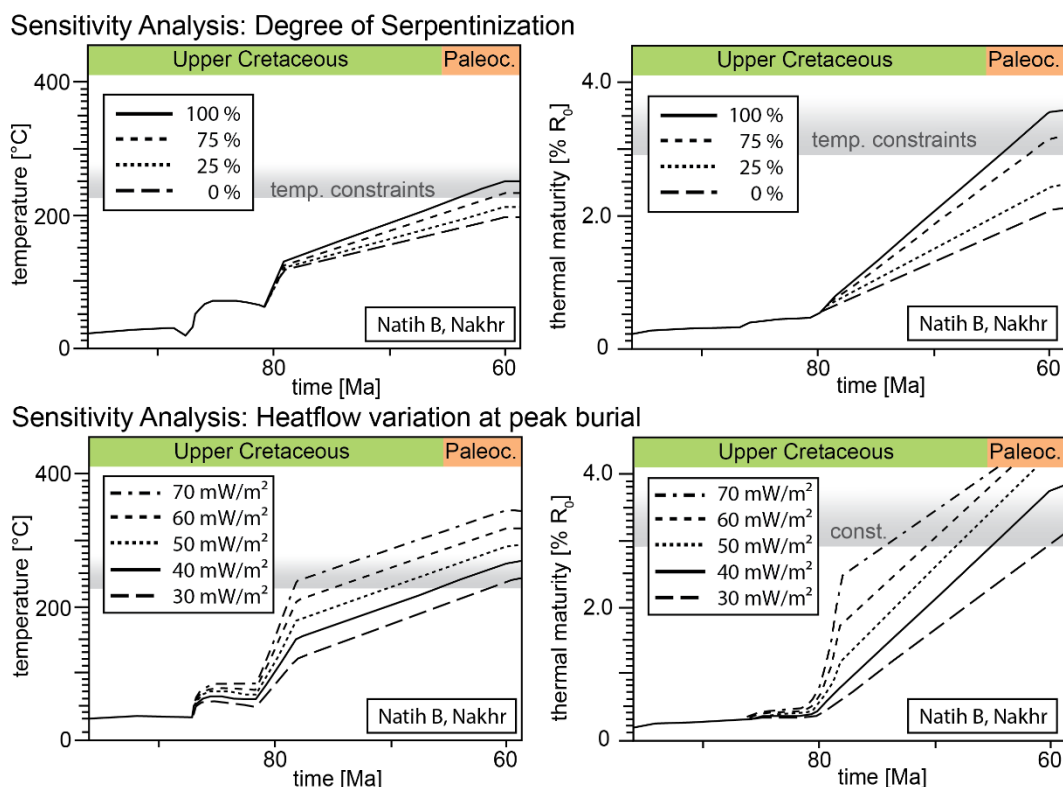
515

516

517

To restore the former minimum thickness of the Semail Ophiolite, the thickness of the Hawasina Nappes along the transect was fixed to 2 km, as suggested by the maximum present-day thickness of the Jebel Misht exotics. To reach the required thermal conditions measured at the entrance of the Wadi Nakhr (Natih B: 2.83-3.72 % VR, 225-260 °C; Grobe et al., 2016), 8-10 km of original, total thickness of strongly serpentinized ophiolite sequence are needed in addition to the 2 km of Hawasina Nappes (Figures 9b and 10b). These thicknesses are also sufficient to reach peak temperatures calculated for older stratigraphy at the northern flank of the Jebel Akhdar Dome (Shu'aiba Fm. at Wadi Yiqah: 270-295 °C by RSCM, Figures 9c and 10c). Modeling results show an earlier heating and more rapid increase in maturity in the north. We associate this with the 2 Mys earlier onset of obduction and, hence, a longer burial of the northern carbonate platform (Wadi Yiqah) under the active ophiolite obduction compared to its southern counterpart (Béchenec et al., 1990; Cowan et al., 2014).

518 Another factor influencing the modeling results is related to the lithology of the overburden and its compaction.
519 In the special case of burial under an ophiolite, serpentinization of peridotite and its impact on ophiolite density
520 and thermal conductivity must be considered. Sensitivity analysis of ophiolite serpentinization shows the
521 temperature and thermal maturity effects on our model (Figure 11). A model-case of ophiolite without any
522 serpentinized peridotite (0 %-case, $\rho_{\text{ophio}}=3133 \text{ kg/m}^3$) would represent the largest deviation compared to our best-
523 case model assuming complete ophiolite serpentinization (100 %-case, $\rho_{\text{ophio}}=3069 \text{ kg/m}^3$). This density is based
524 on Al-Lazki et al. (2002). Even if the upper part of the ophiolite was missing in the Jebel Akhdar area (Nicolas
525 and Boudier, 2015), this and the field data of Searle and Cox (2002) in the Saih Hatat support strong
526 serpentinization. A less serpentinized ophiolite means higher densities and related higher thermal conductivities
527 of the overburden and thus lower peak temperatures in the sediments below. In the case of no serpentinization,
528 peak temperature of Natih B in the Wadi Nakhr would decrease by c. $60 \text{ }^\circ\text{C}$ resulting in a maximum thermal
529 maturity decrease of 1.5 % VR. The best fit model with an ophiolite thickness of 8-10 km would need additional
530 3 km of overburden at 0 % serpentinization to equally match the measured thermal maturities. Additional
531 thicknesses of 0.75 km (75 % serpentinization), 1.5 km (50 % serpentinization) and 2.25 km (25 %
532 serpentinization) apply for lower degrees of serpentinization, respectively (compare Fig. 9).
533 Results depend strongly on basal heat flow (Figure S3). The best fit model of 40 mW/m^2 at maximum burial is
534 typical for a passive continental margin setting. If this heat flow at peak burial would be lowered to 30 mW/m^2 an
535 additional amount of 1.2 km of ophiolitic overburden would be required to achieve a match with thermal
536 calibration data (Figure 11). Increased heat flow values to 50, 60 or 70 mW/m^2 would result in lowering of
537 overburden by 1.3, 2.4 and 3.5 km , respectively (Figure 11).
538



539
540 **Figure 11: Sensitivity analysis: Top: Different degrees of serpentinization of the peridotite within the Semail Ophiolite**
541 **affect the temperature (left) and thermal maturity (right) evolution (modeled for Natih B Fm. at Wadi Nakhr). Pure**
542 **peridotite (0 % serpentinization) require additional 3 km of ophiolite in addition to the 8-10 km of the best-fit model**

543 to equally match the calibration data. 100 % refers to complete serpentinization of the peridotite in the ophiolite.
544 Bottom: The influence of variable heat flow values at peak burial on temperature (left) and thermal maturity (right).

545 5. Discussion

546 Evaluating uncertainties in basin and petroleum system models is especially important for complex areas such as
547 the Jebel Akhdar, where sedimentary rocks reached high temperatures and maturities due to deep and rapid burial.
548 In the following, we discuss these uncertainties with respect to temperature and burial history, overpressure build-
549 up and induced fluid flow. For all presented basin models of the study area, the following assumptions apply: (1)
550 decompacting the present-day lithologies does not consider rock volume lost by pressure solution. This is probably
551 of minor importance in our study area as host-rock buffered isotope ratios of the veins were interpreted as local
552 sinks for nearby dissolved calcite (Arndt et al., 2014; Hilgers et al., 2006), so that the overall rock volume remains
553 approximately constant, (2) decompaction only accounts for burial, whereas a possible tectonic compaction is
554 neglected (Neumaier, 2015) and (3) calculated overpressure does not include a rock volume decrease due to
555 pressure solution.

556 5.1. Burial history

557 Little is known about the very early phase of burial, before 91 Ma (Figures 6 and 7, Grobe et al., 2018). The
558 assumptions for this period are based on hypotheses on the tectonic evolution of the passive continental margin
559 as well as data on thickness of sedimentary units but are not strongly constrained by petrographical-geological
560 data.

561 In Turonian times (Robertson, 1987) a southwest-ward-moving forebulge, related to plate convergence, affected
562 northern Oman. It eroded the northeastern platform edge and migrated southwest-ward to the present-day position
563 of the Adam Foothills (Robertson, 1987). Measured thermal maturities of 1.1 % VR_r were used to reconstruct
564 peak temperatures during burial in Jebel Qusaybah, Adam Foothills to c. 140 °C. Numerical basin modeling
565 results reveal that additional paleo-overburden of at least maximum 4 to 4.5 km (Natih B, Qusaybah, Figure 10)
566 is required to reach these temperatures. The exhumation history of the Adam Foothills is not well known; our
567 model is based on an interpreted late exhumation during the Miocene (Claringbould et al., 2013). Earlier
568 exhumation would shorten the time span of the rock at higher temperatures (Figure 7), lead to decreased thermal
569 maturity and, hence, would require additional overburden to match the measured thermal maturity data. Therefore,
570 the resulting burial of 4 to 4.5 km has to be regarded as minimum value. South of the Adam Foothills basin
571 geometries do not show tilting and are interpreted as not affected by the moving foredeep. Here peak burial was
572 reached under c. 3 km of Fiqa, Hadhramaut and Fars formations. This is based on the assumption that present-day
573 burial equals deepest burial as no thermal calibration data of the area south of Jebel Qusaybah was-are
574 availableachieved, which is in agreement with interpretations of Terken (1999) and Warburton et al. (1990).

575 In case of the Jebel Akhdar, peak temperatures were reached as a consequence of burial below the ophiolite
576 (Loosveld et al., 1996; Searle et al., 2003; Searle, 2007; Warren et al., 2005). Here the sedimentary rocks reached
577 high temperatures and maturities as shown by solid bitumen reflectance, RSCM, FT-IR and Rock-Eval pyrolysis
578 data (Fink et al., 2015; Grobe et al., 2016). Pre-obduction burial by sedimentation is not sufficient for such high
579 thermal maturities, and it likewise cannot be explained by increased basal heat flow before 91 Ma or after 55 Ma.
580 Influence of local hydrothermal effects cannot be excluded, but because the entire Jebel Akhdar reached high

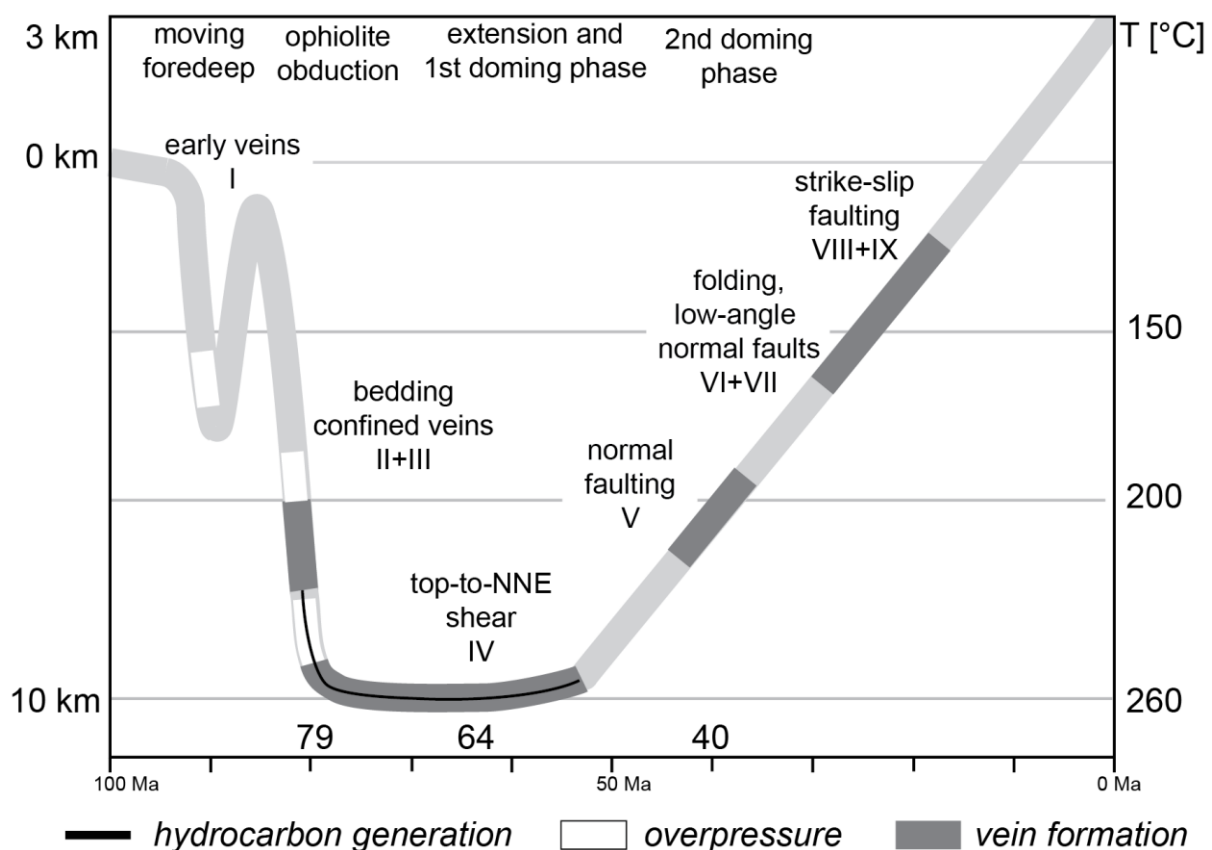
581 temperatures, short-term, local events are unlikely to have been dominant. A regional thermal overprint on the
582 passive margin sediments by warm ophiolite obduction can be excluded and is hence not accounted for in the
583 model. Due to the at least 2 km thick imbricated Hawasina Nappes between the ophiolite and the passive margin
584 sequence, the thermal overprint did not affect the top of the carbonate platform. Limited thermal overprint of the
585 units underlying the ophiolite is supported by the fact that the sediments of the nappes directly below the ophiolite
586 do not show signs of regional metamorphism in the Jebel Akhdar region (Searle, 1985). This is in agreement with
587 models of Lutz et al. (2004). Moreover, the thermal imprint as observed by the metamorphic sole in northern
588 Oman only affects 10's of meters in the sub-thrust Hawasina Nappes (Searle and Cox, 2002) and not the carbonate
589 platform sediments below. This minor overprint is also observed in other areas (e.g. Wygrala, 1989).

590 To reach the measured maturity values in the Jebel Akhdar, a paleo-thickness of the ophiolite in the order of 8-
591 10 km on top of 2 km of Hawasina Nappes is required (Figure 10); this corresponds to 280 to ~~320-340~~ MPa of
592 lithostatic pressure, in rough agreement with the pressure reconstructed by combining fluid inclusion data and
593 independently determined thermal rock maturity temperatures (cf. FI results: 254 ± 30 MPa).

594 Basin modeling indicates that highest temperatures were reached much later than deepest burial under the ophiolite
595 (Figure 7), directly prior to uplift-exhumation. This difference is interpreted as the time the rock advection needs
596 to heat the rock needed for thermal equilibration after rapid burial. Deep burial under the ophiolite represents the
597 only time in the basin's evolution when ductile limestone deformation was possible (Grobe et al., 2018). However,
598 there is uncertainty concerning the exact timing of deepest burial in the Jebel Akhdar (we used 79 Ma according
599 to U-Pb dating of eclogites in the Saih Hatat window; Warren et al., 2005), the related basal heat flow (discussion,
600 Fig. S2) and the beginning of early uplift-exhumation (we used 55 Ma, as discussed below). A later exhumation
601 would not be sufficient to match observed thermal maturities with thermometry data. The slightly higher
602 temperatures of the model compared to thermometry data suggest that an even quicker exhumation might have
603 taken place.

604 Our peak temperatures are in agreement with temperatures of c. 200 °C suggested for the top of the carbonate
605 platform by Breton et al. (2004), ~~and~~ non-reset zircon fission tracks in the pre-Permian basement indicating peak
606 temperatures up to 280 °C (Saddiqi et al., 2006), and ductile limestone conditions observed at the Jurassic-
607 Cretaceous boundary (Grobe et al., 2018, Figure 7). Moreover, thermal maturities of the same stratigraphic units
608 show similar values along the transect and around the dome (Grobe et al., 2016). Hence, we assume a similar
609 burial history for the entire Jebel Akhdar and were able to refine previous models (Grobe et al., 2016) with the
610 here presented larger dataset. The temperatures used in our models are in contrast with recent results on mixed
611 layers illite-smectite ~~layers~~ and clay mineral assemblages from the Jebel Akhdar by Aldega et al. (2017) who
612 argue for peak temperatures of 150-200 °C on the northern flank of the Jebel Akhdar and 120-150 °C on the
613 southern flank. These values are incompatible with our solid bitumen and Raman spectroscopy data, as well as
614 with the overmature Natih B source rock on the southern flank (data presented here and in Grobe et al., 2016).
615 Independent data on temperatures from fluid inclusions confirm the higher temperature range. At present, there is
616 no clear explanation for this discrepancy. However, it has been shown that the vitrinite reflectance system is more
617 sensitive to rapid temperature changes than clay mineralogy (e.g. Hillier et al., 1995; Velde and Lanson, 1993). If
618 burial was short enough, the clay minerals may not have time to recrystallize, possibly due to a lack of potassium,
619 whereas vitrinite reflectance increases. Alternatively, we speculate that the clay minerals were transformed during
620 top-to-NNE shearing, thus their state do not show peak burial. Indeed it has been shown that deformation

621 associated with this early extension reaches deeply into the passive margin sequence, and includes the Rayda and
 622 Shuaiba Formations (Grobe et al., 2018; Mattern and Scharf, 2018). Furthermore, Aldega et al. (2017) argue that
 623 the cooling history proposed by Grobe et al. (2016) indicates temperature in the basement $< 70^{\circ}\text{C}$ during the
 624 Eocene-Oligocene, thus not accounting for thermochronological data in pre-Permian basement rocks. In fact, the
 625 calibration data we used for the basement indicate rapid cooling at 55 ± 5 Ma (Poupeau et al., 1998; Saddiqi et
 626 al., 2006), in agreement with models of Grobe et al. (2016) and the exhumation presented in this work.
 627 This exhumation might be a result of the ductile top-to-NNE shearing event (64 ± 4 Ma, Hansman et al., 2018;
 628 Grobe et al., 2018). Its onset marks the time-exhumation of the carbonate platform after of deepest burial, and r
 629 Related peak temperatures measured in fluid inclusions of bedding parallel veins estimated-were estimated to at
 630 $186\text{--}221^{\circ}\text{C}$ by Holland et al. (2009) assuming an ophiolitic overburden of 5 km (Sahtan Fm., Wadi Nakhr). If we
 631 adjust this pressure correction for higher values of 280 to 340 MPa accounting for the here elaborated 8 to 10 km
 632 of ophiolite and 2 km of sedimentary nappes, trapping temperatures would increase to c. $296\text{--}364^{\circ}\text{C}$ (Table 3),
 633 which are in the order of the maximum burial temperatures as deduced from organic matter maturity.
 634 **Figure 12** presents a summary burial graph integrating all presented data in a plot of the temperature evolution
 635 over time. Highlighted in gray is a additional pressure data is gained by fluid inclusion thermometry. These data
 636 indicate paleo-fluid temperatures in the range of $225 \pm 4^{\circ}\text{C}$ (280 MPa) to $266 \pm 5^{\circ}\text{C}$ (340 MPa) during burial
 637 under the ophiolite (bedding-confined veins), c. $296\text{--}364^{\circ}\text{C}$ at peak burial (top-to-NNE sheared veins) and
 638 $213 \pm 3^{\circ}\text{C}$ during exhumation with a later phase of primary inclusion outlining 184 ± 3 to $189 \pm 7^{\circ}\text{C}$ (both strike-
 639 slip related veins). Temperature decrease within the latter formed parts of the strike-slip veins might relate to a
 640 change of fluid source or to exhumation during vein formation. In combination with our thermochronology data
 641 the second possibility appears more likely and would imply strike-slip faults developed after c. 55 Ma.
 642



644 **Figure 12: Summary sketch of burial and exhumation for the top of the carbonate platform (Natih Fm.) integrating all**
645 **presented datasets. Headings refer to the tectonic phases and captions to the structural generations I-IX (Grobe et al.,**
646 **2018) and. Shown as Ages reflect deepest burial reached at c. 79 Ma, the onset of initial dome formation at 64 Ma (top-**
647 **to-NNE shearing) and rapid exhumation active at 40 Ma. Temperatures are based on RSCM and FI thermometry, and**
648 **the, pPressure at peak burial data is is calculated out-offrom FI measurements and independently determined**
649 **temperature data to $p_0 = 254 \pm 30$ MPa and $p_L = 340$ MPa. The exhumation history is reconstructed from ZHe ages. (***
650 **indicate times of overpressure formation, gray areas depict vein formation)**

651 5.2. Exhumation history

652 Our new thermochronology data from the central part of the Jebel Akhdar Dome suggest cooling below the reset
653 temperature of the ZHe thermochronometer (c. 130-170 °C) between 48.7 ± 1.8 and 39.8 ± 3.0 Ma (Table 2,
654 Figure 4). The small variation in cooling ages for the different stratigraphic levels indicates rapid passage of the
655 entire rock suite through the ZHe partial retention zone, and consequently rapid exhumation of the Jebel Akhdar
656 Dome. This Eocene cooling is in agreement with ZHe ages of pre-Permian strata of Hansman et al. (2017) ranging
657 between 62 ± 3 and 39 ± 2 Ma. Apatite fission track (AFT) ages measured in the basement of the Jebel Akhdar
658 range between 55 ± 5 Ma and 48 ± 7 Ma (4 samples, Poupeau et al., 1998) and 51 ± 8 Ma to 32 ± 4 Ma (Hansman
659 et al., 2017). The temperature of resetting the AFT system (i.e. the depth of the base of the partial annealing zone)
660 may vary depending on annealing kinetics. For different apatite crystals this temperature ranges between 100 and
661 120 °C (Carlson et al., 1999; Fitzgerald et al., 2006). Hence, these AFT ages reproduce within error with our ZHe
662 results, despite the fact that both systems are sensitive to different temperature intervals (100-120 °C and 130-
663 170 °C, respectively This supports the interpretation of rapid exhumation of the Jebel Akhdar at c. 55 Ma. Zircon
664 fission track ages witness cooling of the Jebel Akhdar below c. 260 °C between 96 and 70 Ma (Saddiqi et al.,
665 2006). This implies slow cooling thereafter (c. 100° between 70 and 55 Ma) until rapid exhumation at c. 55 Ma.
666 Earlier exhumation would not result in required thermal maturities as exposure of the rock to highest temperatures
667 would be too short for thermal equilibration. A reheating event in the late Miocene is not required to explain the
668 data.

669 Our ZHe data from the Muti Formation and the Hawasina Nappes show a spread in ages, between 173 and 43 Ma,
670 i.e. partly much older than the ages observed in the stratigraphically lower units in the center of the dome.

671 A spread in (U-Th)/He-ages is often observed, and has been attributed to radiation damage density, uneven
672 distribution of mother isotopes in the dated crystal, broken grains, grain chemistry, among other causes (e.g.
673 Flowers et al., 2009; Guenther et al., 2013). Several studies show that samples from sedimentary rocks are
674 particularly prone to spread in ages (e.g. von Hagke et al., 2012; Ketcham et al., 2018; Levina et al., 2014). This
675 is because transported grains are subject to abrasion, which influences age correction for grain geometry and may
676 obscure presence of inclusions within the crystal. Additionally, dated grains can originate from different sources,
677 and thus have a different chemical composition and a different pre-depositional temperature history. This may
678 result in different reset temperatures, and consequently different grains (or grain age populations) represent
679 different thermochronometers.

680 It is difficult to prove the existence of such multiple thermochronometers, as independent parameters indicative
681 for different kinetics have not yet been established. Indeed, statistical analysis of different grain age populations
682 requires dating of multiple grains (e.g. to be 95 % certain that a population representing 5 % of the grains is not
683 missed 117 single grain ages need to be dated, Vermeesch (2004)). In any case, reproducing ages determined in
684 different samples indicates the data is geologically meaningful, i.e. the observed spread is the result of partial
685 resetting and/or different kinetics and not the result of factors independent of the time-temperature history, such

686 as undetected inclusions or external helium implantation. We thus interpret the system as only partially reset,
687 implying these units were not heated above the reset temperature (approximately 130-170 °C) after deposition.
688 This interpretation is corroborated by unreset ZHe ages in the Hawasina Window (**Figure 1**, Csontos, pers. comm.).
689 The top of the Natih Formation ~~has seen~~experienced temperatures above 220 °C. We suggest that this apparent
690 contradiction may be explained by juxtaposition of the colder Muti and Hawasina units against the top of the
691 carbonate platform during extensional top-to-NNE shearing. This implies that at least 50 °C of cooling are
692 associated with post obduction extension, i.e. before doming. A two-stage exhumation history of the Jebel Akhdar
693 Dome has also been inferred from structural data (Grobe et al., 2018; Mattern and Scharf, 2018) and the
694 stratigraphic record (Fournier et al., 2006; Mann et al., 1990). Top-to-NNE shearing is associated with tectonic
695 thinning of the ophiolite (Grobe et al., 2018). This tectonic denudation will also result in cooling, and may explain
696 why so little ophiolite is found in the post-obduction sediments. Additionally, ophiolitic material may have been
697 lost to the Gulf of Oman.

698 **5.3. Pressure evolution**

699 Evolution of pore pressures was modelled (Figures S7 and S8) assuming a seal on top of the Natih Fm.
700 ($k_{\text{Muti}}=10^{-23} \text{ m}^2$). Porosity was lost during Muti deposition in the moving forebulge (top seal) and related burial,
701 the emplacement of the Hawasina Nappes and the ophiolite, which induced compaction and a remaining very low
702 porosity of c. 1 %. Hydrostatic pressure increased with burial under the moving forebulge at 88 Ma to 40 MPa,
703 after Muti deposition to 60 MPa and after ophiolite emplacement to 120 MPa. Calculated pore pressure rise above
704 hydrostatic pressure in response to Hawasina Nappe and ophiolite emplacement.

705 Formation of tensile fractures, as inferred from bedding confined, Mode-I veins in the Natih Fm. (Arndt et al.,
706 2014; Grobe et al., 2018; Holland et al., 2009a; Virgo, 2015), require internal fluid pressures (P_f) exceeding the
707 sum of the stress acting normal on the fracture surface (σ_3) and the tensile stress of the rock (T): $P_f > \sigma_3 + T$,
708 and a differential stress ($\sigma_1 - \sigma_3$) below $4T$ (Secor, 1965). Host-rock buffered vein isotope compositions indicate
709 that the veins were formed by local fluids (Arndt et al., 2014) and, hence, require local overpressure cells.

710 Sensitivity analyses of reduced permeabilities of Muti, Natih and Nahr Umr formations show that overpressure
711 generation, necessary for rock fracturing, requires a very good top seal and also a reduced horizontal permeability
712 of the Natih Fm. of 10^{-23} m^2 (Figure S7 and S8). A top seal on its own is not sufficient for overpressures initiating
713 rock failure. This case results in pore pressures up to 300 MPa within the top Natih and localized overpressures
714 of 195 MPa in front of the obducting ophiolite.

715 All results indicate that without low horizontal permeabilities of the Natih Fm. $\leq 10^{-23} \text{ m}^2$ overpressure cells
716 required for vein formation cannot be generated. The reduced permeabilities in the Natih Fm. are necessary to
717 prevent an early, tectonically-driven horizontal pressure release.

718 **5.4. Fluid migration**

719 Numerical basin modeling shows that rapid burial of sedimentary rocks below the ophiolite (88-80 Ma) caused
720 under-compaction, i.e. a porosity too high with respect to burial depth, and consequent pore pressure increase.
721 Two example model results of fluid migration in front of the obducting ophiolite are shown in the electronic
722 supplement Figure S9. If low permeabilities are assigned to the non-source-rock members of the Natih Fm.,
723 migration will mainly take place within the source rocks and at layer interfaces within the Natih Fm. If the

724 complete Natih Fm. has low permeabilities, fluids will leave the source rock vertically first, before lateral
725 migration localizes along layer boundaries. The pressure gradient between overpressures below the allochthonous
726 nappes and the less deeply buried southern foreland initiates tectonically-driven fluid migration in front of the
727 obducting nappes, an idea that was first introduced by Oliver (1986). Solid bitumen accumulations in black stained
728 calcite veins are in agreement with this interpretation (Fink et al., 2015).
729 Dome formation of the Jebel Akhdar anticline around 55 Ma initiated layer tilting and consequent southward
730 migration of the generated hydrocarbons as observed by secondary low reflective solid bitumen generations in
731 Natih veins and host rocks at the southern flank of the Oman Mountains (Fink et al., 2015; Grobe et al., 2016).

732 **6. Conclusions**

733 This study provides insights into the temperature evolution during obduction, prior to subsequent orogenesis.
734 Arabia's passive continental margin was buried to at least 4 km at times of foredeep migration and afterwards
735 under 8-10 km of Semail Ophiolite and 2 km of sedimentary Hawasina Nappes. Deepest Burial under the
736 ophiolite resulted in peak temperatures of up to 300 °C (Shu'aiba Fm.) with sub-lithostatic pore pressures.
737 Ophiolite obduction and overpressure cells expelled fluids towards the foreland, through matrix and fracture
738 porosity.
739 ZHe data show cooling associated with forebulge migration, as well as with exhumation of the Jebel Akhdar
740 Dome.
741 Exhumation of the Jebel Akhdar Dome took place in two stages. A first stage is associated with top-to-NNE
742 shearing, which is responsible for at least 50 °C of cooling, as witnessed by juxtaposition of units including
743 partially reset ZHe ages against units that experienced more than 220 °C. ZHe data show the second exhumation
744 phase, associated with doming of the Jebel Akhdar occurred between 49 and 39 Ma.

745 **Author contribution**

746 JLU, RL and AG initiated and planned the study. AG planned and carried out fieldwork as well as thermal maturity
747 measurements (VR, solid bitumen reflectance, Raman spectroscopy), structural interpretations and basin
748 modelling. AG, CvH, JU, ID and FW carried out fieldwork and structural interpretations. FW and ID conducted
749 the thermochronological measurements with help of CvH. PM and AG performed fluid inclusion thermometry.
750 AG and CvH prepared the manuscript with contributions from all co-authors.

751 **Acknowledgements**

752 We acknowledge the highly-appreciated help of Donka Macherey (sample preparation, RWTH Aachen), the team
753 of the KU Leuven (fluid inclusion measurements) and Keno Lünsdorf (Raman spectroscopy, Georg-August-
754 University, Göttingen). Sample crushing was realized by the team of SELFRAG, Switzerland. Wiekert Visser and
755 Victoria Sachse are thanked for fruitful discussions; Gösta Hoffmann and Wilfried Bauer of GUTech are thanked
756 for helping with field logistics. We are grateful for comments of Edwin Gnos, Andreas Scharf, Wolf-Christian
757 Dullo and Mark Handy on earlier versions of this manuscript and the reviews of Massimiliano Zattin, Luca
758 Aldega, Bruce Levell and Federico Rossetti.

759 **References**

- 760 Agard, P., Omrani, J., Jolivet, L. and Mouthereau, F.: Convergence history across Zagros (Iran): constraints from
761 collisional and earlier deformation, *Int. J. Earth Sci.*, 94(3), 401–419, doi:10.1007/s00531-005-0481-4, 2005.
- 762 Al-Lazki, A. I., Seber, D., Sandvol, E. and Barazangi, M.: A crustal transect across the Oman Mountains on the
763 eastern margin of Arabia, *GeoArabia*, 7(1), 47–78, 2002.
- 764 Al-Wardi, M. and Butler, R. W. H.: Constrictional extensional tectonics in the northern Oman mountains, its role
765 in culmination development and the exhumation of the subducted Arabian continental margin, *Geol. Soc. London,*
766 *Spec. Publ.*, 272(1), 187–202, doi:10.1144/GSL.SP.2007.272.01.11, 2007.
- 767 Aldega, L., Carminati, E., Scharf, A., Mattern, F. and Al-Wardi, M.: Estimating original thickness and extent of
768 the Semail Ophiolite in the eastern Oman Mountains by paleothermal indicators, *Mar. Pet. Geol.*, 84, 18–33,
769 doi:10.1016/j.marpetgeo.2017.03.024, 2017.
- 770 Aldega, L., Bigi, S., Carminati, E., Trippetta, F., Corrado, S. and Kavooosi, M. A.: The Zagros fold-and-thrust belt
771 in the Fars province (Iran): II. Thermal evolution, *Mar. Pet. Geol.*, 93, 376–390,
772 doi:10.1016/J.MARPETGEO.2018.03.022, 2018.
- 773 Aoya, M., Kouketsu, Y., Endo, S., Shimizu, H., Mizukami, T., Nakamura, D. and Wallis, S.: Extending the
774 applicability of the Raman carbonaceous-material geothermometer using data from contact metamorphic rocks,
775 *J. Metamorph. Geol.*, 28(9), 895–914, doi:10.1111/j.1525-1314.2010.00896.x, 2010.
- 776 Arndt, M., Virgo, S., Cox, S. F. and Urai, J. L.: Changes in fluid pathways in a calcite vein mesh (Natih Fm, Oman
777 Mountains): insights from stable isotopes, *Geofluids*, 14(4), 391–418, doi:10.1111/gfl.12083, 2014.
- 778 Barker, C. E. E. and Pawlewicz, M. J. J.: Calculation of vitrinite reflectance from thermal histories and peak
779 temperatures, in *Vitrinite Reflectance as a Maturity Parameter*, vol. 570, edited by P. Mukhopadhyay and W.
780 Dow, pp. 216–229, American Chemical Society., 1994.
- 781 Béchenec, F., Metour, J. L. E., Rabu, D., Villey, M. and Beurrier, M.: The Hawasina Basin: A fragment of a
782 starved passive continental margin, thrust over the Arabian Platform during obduction of the Sumail Nappe,
783 *Tectonophysics*, 151(1–4), 323–343, doi:10.1016/0040-1951(88)90251-X, 1988.
- 784 Béchenec, F., Le Metour, J., Rabu, D., Bourdillon-de-Grissac, C., de Wever, P., Beurrier, M. and Villey, M.:
785 The Hawasina Nappes: stratigraphy, palaeogeography and structural evolution of a fragment of the south-Tethyan
786 passive continental margin, *Geol. Soc. London, Spec. Publ.*, 49(1), 213–223,
787 doi:10.1144/GSL.SP.1992.049.01.14, 1990.
- 788 Bernoulli, D., Weissert, H. and Blome, C. D.: Evolution of the Triassic Hawasina Basin, Central Oman Mountains,
789 *Geol. Soc. London, Spec. Publ.*, 49(1), 189–202, doi:10.1144/GSL.SP.1992.049.01.12, 1990.
- 790 Beurrier, M., Bechenec, F., Rabu, D. and Hutin, G.: Geological Map of Rustaq - explanatory notes, Sultanat
791 Oman, *Minist. Pet. Miner.*, 1986.
- 792 Beyssac, O., Goffé, B., Chopin, C. and Rouzaud, J. N.: Raman spectra of carbonaceous material in metasediments:
793 A new geothermometer, *J. Metamorph. Geol.*, 20, 859–871, doi:10.1046/j.1525-1314.2002.00408.x, 2002.
- 794 Bodnar, R. J.: Revised equation and table for determining the freezing point depression of H₂O-NaCl solutions,
795 *Gechimica Cosmochim. Acta*, 57, 683–684, 1993.
- 796 Breton, J. P., Béchenec, F., Le Métour, J., Moen-Maurel, L. and Razin, P.: Eoalpine (Cretaceous) evolution of
797 the Oman Tethyan continental margin: Insights from a structural field study in Jabal Akhdar (Oman Mountains),
798 *GeoArabia*, 9(2), 41–58, 2004.

799 Brown, P. E.: FLINCOR; a microcomputer program for the reduction and investigation of fluid-inclusion data,
800 *Am. Mineral.*, 74, 1390–1393, 1989.

801 Van Buchem, F. S. P., Razin, P., Homewood, P. W., Philip, J. M., Eberli, G. P., Platel, J. P., Roger, J., Eschard,
802 R., Desaubliaux, G. M. J., Boisseau, T., Leduc, J. P., Labourdette, R. and Cantaloube, S.: High resolution sequence
803 stratigraphy of the Natih Formation (Cenomanian/Turonian) in northern Oman: distribution of source rocks and
804 reservoir facies, *GeoArabia*, 1(1), 65–91, 1996.

805 Van Buchem, F. S. P., Razin, P., Homewood, P. W., Oterdoom, W. H. and Philip, J.: Stratigraphic organization
806 of carbonate ramps and organic- rich intrashelf basins: Natih Formation (middle Cretaceous) of northern Oman,
807 *Am. Assoc. Pet. Geol. Bull.*, 86(1), 21–53, doi:10.1306/61EEDA30-173E-11D7-8645000102C1865D, 2002.

808 Carlson, W. D., Donelick, R. A. and Ketcham, R. A.: Variability of apatite fission-track annealing kinetics: I.
809 Experimental results, *Am. Mineral.*, 84(9), 1213–1223, doi:10.2138/am-1999-0901, 1999.

810 Claringbould, J. S., Hyden, B. B., Sarg, J. F. and Trudgill, B. D.: Structural evolution of a salt-cored, domed,
811 reactivated fault complex, Jebel Madar, Oman, *J. Struct. Geol.*, 51, 118–131, doi:10.1016/j.jsg.2013.03.001, 2013.

812 Coleman, R. G.: Tectonic Setting for Ophiolite Obduction in Oman, *J. Geophys. Res.*, 86(B4), 2497–2508, 1981.

813 Cooper, D. J. W., Ali, M. Y. and Searle, M. P.: Structure of the northern Oman Mountains from the Semail
814 Ophiolite to the Foreland Basin, *Geol. Soc. London, Spec. Publ.*, 392, 129–153, 2014.

815 Cowan, R. J., Searle, M. P. and Waters, D. J.: Structure of the metamorphic sole to the Oman Ophiolite, Sumeini
816 Window and Wadi Tayyin: implications for ophiolite obduction processes, *Geol. Soc. London, Spec. Publ.*,
817 392(1), 155–175, doi:10.1144/SP392.8, 2014.

818 Deville, E. and Sassi, W.: Contrasting thermal evolution of thrust systems: An analytical and modeling approach
819 in the front of the western Alps, *Am. Assoc. Pet. Geol. Bull.*, 90(6), 887–907, doi:10.1306/01090605046, 2006.

820 Duretz, T., Agard, P., Yamato, P., Ducassou, C. C. C., Burov, E. B. and Gerya, T. V.: Thermo-mechanical
821 modeling of the obduction process based on the Oman Ophiolite case, *Gondwana Res.*,
822 doi:10.1016/j.gr.2015.02.002, 2015.

823 Ferreiro Mählmann, R.: Correlation of very low grade data to calibrate a thermal maturity model in a nappe
824 tectonic setting, a case study from the Alps, *Tectonophysics*, 334, 1–33, 2001.

825 Filbrandt, J. B., Al-Dhahab, S., Al-Habsy, A., Harris, K., Keating, J., Al-mahruqi, S., Ozkaya, S. I., Richard, P.
826 D. and Robertson, T.: Kinematic interpretation and structural evolution of North Oman, Block 6, since the Late
827 Cretaceous and implications for timing of hydrocarbon migration into Cretaceous reservoirs, *GeoArabia*, 11(1),
828 97–115, 2006.

829 Fink, R., Virgo, S., Arndt, M., Visser, W., Littke, R. and Urai, J. L. L.: Solid bitumen in calcite veins from the
830 Natih Formation in the Oman Mountains: multiple phases of petroleum migration in a changing stress field, *Int.*
831 *J. Coal Geol.*, 157, 39–51, doi:10.1016/j.coal.2015.07.012, 2015.

832 Fitzgerald, P. G., Baldwin, S. L., Webb, L. E. and O’Sullivan, P. .: He data from slowly cooled crustal terranes
833 and the interpretation of intra-sample variations of single crystal apatite ages from vertical profiles., *Chem. Geol.*,
834 225, 91–120, 2006.

835 Flowers, R. M., Ketcham, R. A., Shuster, D. L. and Farley, K. A.: Apatite (U–Th)/He thermochronometry using
836 a radiation damage accumulation and annealing model, *Geochim. Cosmochim. Acta*, 73(8), 2347–2365,
837 doi:10.1016/J.GCA.2009.01.015, 2009.

838 Forbes, G. A., Jansen, H. S. M. and Schreurs, J.: *Lexicon of Oman - Subsurface Stratigraphy - Reference Guide*

839 to the Stratigraphy of Oman's Hydrocarbon Basins, *GeoArabia Spec. Publ.* 5, 2010.

840 Fournier, M., Lepvrier, C., Razin, P. and Jolivet, L.: Late Cretaceous to Paleogene post-obduction extension and
841 subsequent Neogene compression in the Oman Mountains, *GeoArabia*, 11(4), 17–40, 2006.

842 Glennie, K. W., Boeuf, M. G. A., Clarke, M. W. H., Moody-Stuart, M., Pilaar, W. F. H. and Reinhardt, B. M.:
843 Late Cretaceous Nappes in Oman Mountains and Their Geologic Evolution : Reply, *Am. Assoc. Pet. Geol. Bull.*,
844 57(1), 5–27, 1973.

845 Glennie, K. W., Boeuf, M. G. A., Hughes Clarke, M. W., Moody-Stuart, M., Pilaar, W. F. H. and Reinhardt, B.
846 M.: Geology of the Oman Mountains, *Verh. van het K. Ned. Geol. Mijnbouwkd. Genoot.*, 31, 432, 1974.

847 Gnos, E. and Peters, T.: K-Ar ages of the metamorphic sole of the Semail Ophiolite: implications for ophiolite
848 cooling history, *Contrib. to Mineral. Petrol.*, 113, 325–332, 1993.

849 Goldstein, R. H.: Fluid inclusions in sedimentary and diagenetic systems, *Lithos*, 55(1–4), 159–193,
850 doi:10.1016/S0024-4937(00)00044-X, 2001.

851 Gomez-Rivas, E., Bons, P. D., Koehn, D., Urai, J. L., Arndt, M., Virgo, S., Laurich, B., Zeeb, C., Stark, L. and
852 Blum, P.: The Jabal Akhdar Dome in the Oman mountains: Evolution of a dynamic fracture system, *Am. J. Sci.*,
853 314(7), 1104–1139, doi:10.2475/07.2014.02, 2014.

854 Grelaud, C., Razin, P., Homewood, P. W. and Schwab, a. M.: Development of Incisions on a Periodically
855 Emergent Carbonate Platform (Natih Formation, Late Cretaceous, Oman), *J. Sediment. Res.*, 76(4), 647–669,
856 doi:10.2110/jsr.2006.058, 2006.

857 Grobe, A., Littke, R., Urai, J. L. J. L. L., Lünsdorf, N. K. K., Littke, R. and Lünsdorf, N. K. K.: Hydrocarbon
858 generation and migration under a large overthrust: The carbonate platform under the Semail Ophiolite, Jebel
859 Akhdar, Oman, *Int. J. Coal Geol.*, 168, 1–17, doi:10.1016/j.coal.2016.02.007, 2016.

860 Grobe, A., Virgo, S., von Hagke, C., Urai, J. L. L. and Littke, R.: Multiphase Structural Evolution of a Continental
861 Margin During Obduction Orogeny: Insights From the Jebel Akhdar Dome, Oman Mountains, *Tectonics*, 37(3),
862 888–913, doi:10.1002/2016TC004442, 2018.

863 Guenther, W. R., Reiners, P. W., Ketcham, R. A., Nasdala, L. and Giester, G.: *American Journal of Science*, *Am.*
864 *J. Sci.*, 313(March), 145–198, doi:10.2475/03.2013.01, 2013.

865 Habsi, N. Al, Shukaili, M. Al, Tooqi, S. Al, Ehrenberg, S. N. and Bernecker, M.: Lithofacies, diagenesis and
866 reservoir quality of Upper Shu'aiba reservoirs in northwestern Oman, *GeoArabia*, 19(4), 145–182, 2014.

867 Hacker, B. R. and Mosenfelder, J. L.: Metamorphism and deformation along the emplacement thrust of the Semail
868 ophiolite, Oman, *Earth Planet. Sci. Lett.*, 144(3–4), 435–451, doi:10.1016/S0012-821X(96)00186-0, 1996.

869 Hacker, B. R., Mosenfelder, J. L. and Gnos, E.: Rapid emplacement of the Oman ophiolite: Thermal and
870 geochronologic constraints, *Tectonics*, 15(6), 1230–1247, 1996.

871 von Hagke, C., Cederbom, C. E., Oncken, O., Stöckli, D. F., Rahn, M. K. and Schlunegger, F.: Linking the
872 northern Alps with their foreland: The latest exhumation history resolved by low-temperature thermochronology,
873 *Tectonics*, 31(5), n/a-n/a, doi:10.1029/2011TC003078, 2012.

874 Hanna, S. S.: The Alpine deformation of the Central Oman Mountains, *Geol. Soc. London, Spec. Publ.*, 49(1),
875 341–359, doi:10.1144/GSL.SP.1992.049.01.21, 1990.

876 Hansman, R. J., Ring, U., Thomson, S. N. and Brok, B. Den: Late Eocene uplift of the Al Hajar Mountains, Oman,
877 supported by stratigraphy and low-temperature thermochronology, *Tectonics*, doi:10.1002/2017TC004672, 2017.

878 Hansman, R. J., Albert, R., Gerdes, A. and Ring, U.: Absolute ages of multiple generations of brittle structures by

879 U-Pb dating of calcite, *Geology*, doi:10.1130/G39822.1, 2018.

880 Hassanzadeh, J. and Wernicke, B. P.: The Neotethyan Sanandaj-Sirjan zone of Iran as an archetype for passive
881 margin-arc transitions, *Tectonics*, 25(3), 586–621, doi:10.1002/2015TC003926, 2016.

882 Hilgers, C., Kirschner, D. L., Breton, J. P. P. and Urai, J. L.: Fracture sealing and fluid overpressures in limestones
883 of the Jabal Akhdar dome, Oman mountains, *Geofluids*, 6(2), 168–184, doi:10.1111/j.1468-8123.2006.00141.x,
884 2006.

885 Hillier, S., Mátyás, J., Matter, A. and Vasseur, G.: Illite/smectite diagenesis and its variable correlation with
886 vitrinite reflectance in the Pannonian Basin, *Clays Clay Miner.*, 43(2), 174–183,
887 doi:10.1346/CCMN.1995.0430204, 1995.

888 Holland, M., Urai, J. L., Muchez, P. and Willemsse, E. J. M.: Evolution of fractures in a highly dynamic thermal,
889 hydraulic, and mechanical system - (I) Field observations in Mesozoic Carbonates, Jabal Shams, Oman
890 Mountains, *GeoArabia*, 14(1), 57–110, 2009a.

891 Holland, M., Saxena, N. and Urai, J. L.: Evolution of fractures in a highly dynamic thermal, hydraulic, and
892 mechanical system - (II) Remote sensing fracture analysis, Jabal Shams, Oman mountains, *GeoArabia*, 14(3),
893 163–194, 2009b.

894 Homewood, P., Razin, P., Grélaud, C., Droste, H., Vahrenkamp, V., Mettraux, M. and Mattner, J.: Outcrop
895 sedimentology of the Natih Formation, northern Oman: A field guide to selected outcrops in the Adam Foothills
896 and Al Jabal al Akhdar areas, *GeoArabia*, 13(3), 39–120, 2008.

897 Immenhauser, A. and Scott, R. W.: An estimate of Albian sea-level amplitudes and its implication for the duration
898 of stratigraphic hiatuses, *Sediment. Geol.*, 152(1–2), 19–28, doi:10.1016/S0037-0738(02)00260-9, 2002.

899 Immenhauser, A., Schlager, W., Burns, S. J., Scott, R. W., Geel, T., Lehmann, J., van der Gaast, S. and Bolder-
900 Schrijver, L. J. A. J. a.: Late Aptian to late Albian sea-level fluctuations constrained by geochemical and biological
901 evidence (Nahr Umr Formation, Oman), *J. Sediment. Res.*, 69(2), 434–446, doi:10.2110/jsr.69.434, 1999.

902 Jacobs, J., Thomas, R. J., Ksienzyk, A. K. and Dunkl, I. I.: Tracking the Oman Ophiolite to the surface - New
903 fission track and (U-Th)/He data from the Aswad and Khor Fakkan Blocks, United Arab Emirates,
904 *Tectonophysics*, 644, 68–80, doi:10.1016/j.tecto.2014.12.018, 2015.

905 Jirman, P., Geršlová, E., Kalvoda, J. and Melichar, R.: 2d basin modelling in the eastern variscan fold belt (Czech
906 Republic): influence of thrusting on patterns of thermal maturation, *J. Pet. Geol.*, 41(2), 175–188,
907 doi:10.1111/jpg.12699, 2018.

908 De Keijzer, M., Hillgartner, H., Al Dhahab, S. and Rawnsley, K.: A surface-subsurface study of reservoir-scale
909 fracture heterogeneities in Cretaceous carbonates, North Oman, *Geol. Soc. London, Spec. Publ.*, 270(1), 227–244,
910 doi:10.1144/GSL.SP.2007.270.01.15, 2007.

911 Ketcham, R. A.: Forward and Inverse Modeling of Low-Temperature Thermochronometry Data, *Rev. Mineral.*
912 *Geochemistry*, 58, 275–314, doi:10.2138/rmg.2005.58.11, 2005.

913 Ketcham, R. A., Mora, A. and Parra, M.: Deciphering exhumation and burial history with multi-sample down-
914 well thermochronometric inverse modelling, *Basin Res.*, 30, 48–64, doi:10.1111/bre.12207, 2018.

915 Koehrer, B., Zeller, M., Aigner, T., Poepplreiter, M., Milroy, P., Forke, H. and Al-Kindi, S.: Facies and
916 stratigraphic framework of a Khuff outcrop equivalent: Saiq and Mahil formations, Al Jabal al-Akhdar, Sultanate
917 of Oman, *GeoArabia*, 15(2), 91–156, 2010.

918 Koehrer, B., Aigner, T. and Poppelreiter, M.: Field-scale geometries of Upper Khuff reservoir geobodies in an

919 outcrop analogue (Oman Mountains, Sultanate of Oman), *Pet. Geosci.*, 17(1), 3–16, doi:10.1144/1354-079310-
920 009, 2011.

921 Kouketsu, Y., Mizukami, T., Mori, H., Endo, S., Aoya, M., Hara, H., Nakamura, D. and Wallis, S.: A new
922 approach to develop the Raman carbonaceous material geothermometer for low-grade metamorphism using peak
923 width, *Isl. Arc*, 23, 33–50, doi:10.1111/iar.12057, 2014.

924 Levina, M., Horton, B. K., Fuentes, F. and Stockli, D. F.: Cenozoic sedimentation and exhumation of the foreland
925 basin system preserved in the Precordillera thrust belt (31-32°S), southern central Andes, Argentina, *Tectonics*,
926 33(9), 1659–1680, doi:10.1002/2013TC003424, 2014.

927 Lippard, S. J., Smewing, J. D., Rothery, D. a. and Browning, P.: The geology of the Dibba zone, northern Oman
928 mountains - a preliminary study, *J. Geol. Soc. London.*, 139(1), 59–66, doi:10.1144/gsjgs.139.1.0059, 1982.

929 Loosveld, R. J. H., Bell, A. and Terken, J. J. M.: The Tectonic Evolution of Interior Oman, *GeoArabia*, 1(1), 28–
930 51 [online] Available from: [http://search.ebscohost.com/login.aspx?direct=true&db=geh&AN=1998-](http://search.ebscohost.com/login.aspx?direct=true&db=geh&AN=1998-061521&site=ehost-live&scope=cite)
931 061521&site=ehost-live&scope=cite, 1996.

932 Lünsdorf, N. K.: Raman spectroscopy of dispersed vitrinite - methodical aspects and correlation with reflectance,
933 *Int. J. Coal Geol.*, 153(1), 75–86, doi:10.1016/j.coal.2015.11.010, 2016.

934 Lünsdorf, N. K., Dunkl, I., Schmidt, B. C., Rantitsch, G. and von Eynatten, H.: The thermal history of the Steinach
935 Nappe (eastern Alps) during extension along the Brenner Normal Fault system indicated by organic maturation
936 and zircon (U-Th)/ He thermochronology, *Austrian J. Earth Sci.*, 105(3), 17–25, 2012.

937 Lünsdorf, N. K., Dunkl, I., Schmidt, B. C., Rantitsch, G. and von Eynatten, H.: Towards a Higher Comparability
938 of Geothermometric Data Obtained by Raman Spectroscopy of Carbonaceous Material. Part 2: A Revised
939 Geothermometer, *Geostand. Geoanalytical Res.*, 41(4), 593–612, doi:10.1111/ggr.12178, 2017.

940 Mair, D., Lechmann, A., Herwegh, M., Nibourel, L. and Schlunegger, F.: Linking Alpine deformation in the Aar
941 Massif basement and its cover units – the case of the Jungfrau–Eiger mountains (Central Alps, Switzerland), *Solid*
942 *Earth*, 9(5), 1099–1122, doi:10.5194/se-9-1099-2018, 2018.

943 Mann, a., Hanna, S. S. and Nolan, S. C.: The post-Campanian tectonic evolution of the Central Oman Mountains:
944 Tertiary extension of the Eastern Arabian Margin, *Geol. Tectonics Oman Reg.*, 49(1), 549–563,
945 doi:10.1144/gsl.sp.1992.049.01.33, 1990.

946 Mashhadi, Z. S., Rabbani, A. R. and Kamali, M. R.: Geochemical characteristics and hydrocarbon generation
947 modeling of the Kazhdumi (Early Cretaceous), Gurpi (Late Cretaceous) and Pabdeh (Paleogene) formations,
948 Iranian sector of the Persian Gulf, *Mar. Pet. Geol.*, 66, 978–997, doi:10.1016/J.MARPETGEO.2015.08.008, 2015.

949 Mattern, F. and Scharf, A.: Postobductional extension along and within the Frontal Range of the Eastern Oman
950 Mountains, *J. Asian Earth Sci.*, 154, doi:10.1016/j.jseaes.2017.12.031, 2018.

951 Le Metour, J., Rabu, D., Tegye, M., Bechenec, F., Beurrier, M. and Villey, M.: Subduction and obduction: two
952 stages in the EoAlpine tectonometamorphic evolution of the Oman Mountains, *Geol. Soc. London, Spec. Publ.*,
953 49(1), 327–339, doi:10.1144/GSL.SP.1992.049.01.20, 1990.

954 Mouthereau, F.: Timing of uplift in the Zagros belt/Iranian plateau and accommodation of late Cenozoic Arabia -
955 Eurasia convergence, *Geol. Mag.*, 148(5–6), 726–738, doi:10.1017/S0016756811000306, 2011.

956 Mozafari, M., Swennen, R., Balsamo, F., Clemenzi, L., Storti, F., El Desouky, H., Vanhaecke, F., Tueckmantel,
957 C., Solum, J. and Taberner, C.: Paleofluid Evolution In Fault-Damage Zones: Evidence From Fault-Fold
958 Interaction Events In the Jabal Qusaybah Anticline (Adam Foothills, North Oman), *J. Sediment. Res.*, 85(12),

959 1525–1551, doi:10.2110/jsr.2015.95, 2015.

960 Muchez, P., Marshall, J. D., Touret, J. L. R. and Viaene, W. a.: Origin and migration of palaeofluids in the Upper
961 Viséan of the Campine Basin, northern Belgium, *Sedimentology*, 41(1), 133–145, doi:10.1111/j.1365-
962 3091.1994.tb01395.x, 1994.

963 Neumaier, M.: Structural Restoration and Basin and Petroleum Systems Modeling: Case Studies from the
964 Monagas Fold and Thrust Belt, Venezuela and the Moroccan Atlantic Margin, Dissertation, RWTH Aachen
965 University., 2015.

966 Nibourel, L., Berger, A., Egli, D., Luensdorf, N. K. and Herwegh, M.: Large vertical displacements of a crystalline
967 massif recorded by Raman thermometry, *Geology*, 46(10), 879–882, doi:10.1130/G45121.1, 2018.

968 Nicolas, A. and Boudier, F. F.: Structural contribution from the Oman ophiolite to processes of crustal accretion
969 at the East Pacific Rise, *Terra Nov.*, 27(2), 77–96, doi:10.1111/ter.12137, 2015.

970 Nolan, S. C., Skelton, P. W., Clissold, B. P. and Smewing, J. D.: Maastrichtian to early Tertiary stratigraphy and
971 palaeogeography of the Central and Northern Oman Mountains, *Geol. Soc. London, Spec. Publ.*, 49(1), 495–519,
972 doi:10.1144/gsl.sp.1992.049.01.31, 1990.

973 Nöth, S., Karg, H. and Littke, R.: Reconstruction of Late Paleozoic heat flows and burial histories at the
974 Rhenohercynian-Subvariscan boundary, Germany, *Int. J. Earth Sci.*, 90(2), 234–256,
975 doi:10.1007/s005310000114, 2001.

976 Oliver, J.: Fluids expelled tectonically from orogenic belts: Their role in hydrocarbon migration and other geologic
977 phenomena, *Geology*, 14(February), 99–102, 1986.

978 Oxburgh, E. R. and Turcotte, D. L.: Thermal gradients and regional metamorphism in overthrust terrains with
979 special reference to the Eastern Alps, *Schweizerische Mineral. und Petrogr. Mitteilungen*, 54(2/3), 642–662, 1974.

980 Philip, J., Borgomano, J. and Al-Maskiry, S.: Cenomanian-Early Turonian carbonate platform of Northern Oman:
981 stratigraphy and palaeo-environments, *Palaeogeogr. Palaeoclimatol. Palaeoecol.*, 119, 77–92, 1995.

982 Pöppelreiter, M. C., Schneider, C. J., Obermaier, M., Forke, H. C., Koehrer, B. and Aigner, T.: Seal turns into
983 reservoir: Sudair equivalents in outcrops, A1 Jabal al-Akhdar, Sultanate of Oman, *GeoArabia*, 16(1), 69–108,
984 2011.

985 Poupeau, G., Saddiqi, O., Michard, A., Goffé, B. and Oberhänsli, R.: Late thermal evolution of the Oman
986 Mountains subophiolitic windows: Apatite fission-track thermochronology, *Geology*, 26(12), 1139–1142, 1998.

987 Pratt, R., Smewing, D., Swansea, S. A., Pratt, B. R. and Smewing, J. D.: Jurassic and Early Cretaceous platform
988 margin configuration and evolution, central Oman Mountains, *Geol. Soc. London, Spec. Publ.*, 49(1), 69–88,
989 doi:10.1144/GSL.SP.1992.049.01.06, 1990.

990 Rabu, D., Le Metour, J., Bechennec, F., Beurrier, M., Villey, M. and Bourdillon-Jeudy de Grissac, C.:
991 Sedimentary aspects of the Eo-Alpine cycle on the northeast edge of the Arabian Platform (Oman Mountains),
992 *Geol. Soc. London, Spec. Publ.*, 49(1), 49–68, doi:10.1144/GSL.SP.1992.049.01.05, 1990.

993 Rantitsch, G. and Rainer, T.: Thermal modeling of Carboniferous to Triassic sediments of the Karawanken Range
994 (Southern Alps) as a tool for paleogeographic reconstructions in the Alpine-Dinaridic-Pannonian realm, *Int. J.*
995 *Earth Sci.*, 92(2), 195–209, doi:10.1007/s00531-003-0312-4, 2003.

996 Reiners, P. W.: Zircon (U-Th)/He Thermochronometry, *Rev. Mineral. Geochemistry*, 58(1936), 151–179,
997 doi:10.2138/rmg.2005.58.6, 2005.

998 Reutter, K.-J., Teichmüller, M. and Teichmüller, R.: The Coalification Pattern in the Northern Apennines and its

999 Palaeogeothermic and Tectonic Significance, *Geol. Rundschau/Geologische Rundschau*, 72(3), 861–894, 1988.

1000 Rioux, M., Bowring, S., Kelemen, P., Gordon, S., Miller, R. and Dudás, F.: Tectonic development of the Semail
1001 ophiolite: High-precision U-Pb zircon geochronology and Sm-Nd isotopic constraints on crustal growth and
1002 emplacement, *J. Geophys. Res. Solid Earth*, 118(5), 2085–2101, doi:10.1002/jgrb.50139, 2013.

1003 Rioux, M., Garber, J., Bauer, A., Bowring, S., Searle, M., Kelemen, P. and Hacker, B.: Synchronous formation of
1004 the metamorphic sole and igneous crust of the Semail ophiolite: New constraints on the tectonic evolution during
1005 ophiolite formation from high-precision U–Pb zircon geochronology, *Earth Planet. Sci. Lett.*, 451, 185–195,
1006 doi:10.1016/j.epsl.2016.06.051, 2016.

1007 Robertson, A.: The transition from a passive margin to an Upper Cretaceous foreland basin related to ophiolite
1008 emplacement in the Oman Mountains, *Geol. Soc. Am. Bull.*, 99, 633–653, doi:10.1130/0016-7606(1987)99<633,
1009 1987.

1010 Rolandone, F., Lucazeau, F., Leroy, S., Mareschal, J.-C., Jorand, R., Goutorbe, B. and Bouquerel, H.: New heat
1011 flow measurements in Oman and the thermal state of the Arabian Shield and Platform, *Tectonophysics*, 589, 77–
1012 89, doi:10.1016/j.tecto.2012.12.034, 2013.

1013 Roure, F., Andriessen, P., Callot, J. P., Faure, J. L., Ferket, H., Gonzales, E., Guilhaumou, N., Lacombe, O.,
1014 Malandain, J., Sassi, W., Schneider, F., Swennen, R., Vilasi, N., Box, P. O., Gonzales, E., Guilhaumou, N.,
1015 Lacombe, O., Malandain, J., Sassi, W., Schneider, F., Swennen, R. and Vilasi, N.: The use of palaeo-thermo-
1016 barometers and coupled thermal, fluid flow and pore-fluid pressure modelling for hydrocarbon and reservoir
1017 prediction in fold and thrust belts, *Geol. Soc. London, Spec. Publ.*, 348(1), 87–114, doi:10.1144/SP348.6, 2010.

1018 Saddiqi, O., Michard, A. N., Goffe, B. R., Poupeau, G. É. and Oberhänsli, R. O.: Fission-track thermochronology
1019 of the Oman Mountains continental windows, and current problems of tectonic interpretation, *Bull. la Soc. Geol.*
1020 *Fr.*, 177(3), 127–143, doi:10.2113/gssgfbull.177.3.127, 2006.

1021 Schito, A., Corrado, S., Trolese, M., Aldega, L., Caricchi, C., Cirilli, S., Grigo, D., Guedes, A., Romano, C.,
1022 Spina, A. and Valentim, B.: Assessment of thermal evolution of Paleozoic successions of the Holy Cross
1023 Mountains (Poland), *Mar. Pet. Geol.*, 80, 112–132, doi:10.1016/J.MARPETGEO.2016.11.016, 2017.

1024 Schito, A., Andreucci, B., Aldega, L., Corrado, S., Di Paolo, L., Zattin, M., Szaniawski, R., Jankowski, L. and
1025 Mazzoli, S.: Burial and exhumation of the western border of the Ukrainian Shield (Podolia): a multi-disciplinary
1026 approach, *Basin Res.*, 30, 532–549, doi:10.1111/bre.12235, 2018.

1027 Scott, R. W.: Chronostratigraphy of the Cretaceous carbonate shelf, southeastern Arabia, *Geol. Soc. London,*
1028 *Spec. Publ.*, 49(1), 89–108, doi:10.1144/GSL.SP.1992.049.01.07, 1990.

1029 Searle, M. P.: Sequence of thrusting and origin of culminations in the northern and central Oman Mountains, *J.*
1030 *Struct. Geol.*, 7(2), 129–143, doi:10.1016/0191-8141(85)90127-0, 1985.

1031 Searle, M. P. and Cox, J. O. N.: Subduction zone metamorphism during formation and emplacement of the Semail
1032 ophiolite in the Oman Mountains, *Geol. Mag.*, 139(03), 241–255, doi:10.1017/S0016756802006532, 2002.

1033 Searle, M. P., Warren, C. J., Waters, D. J. and Parrish, R. R.: Subduction zone polarity in the Oman Mountains:
1034 implications for ophiolite emplacement, *Geol. Soc. London, Spec. Publ.*, 218(1), 467–480,
1035 doi:10.1144/GSL.SP.2003.218.01.24, 2003.

1036 Searle, M. P., Warren, C. J. J., Waters, D. . J. and Parrish, R. . R.: Structural evolution, metamorphism and
1037 restoration of the Arabian continental margin, Saih Hatat region, Oman Mountains, *J. Struct. Geol.*, 26(3), 451–
1038 473, doi:10.1016/j.jsg.2003.08.005, 2004.

1039 Searle, M. P. M. P.: Structural geometry, style and timing of deformation in the Hawasina Window, Al Jabal al
1040 Akhdar and Saih Hatat culminations, Oman Mountains, *GeoArabia*, 12(2), 99–130, 2007.

1041 Secor, D. T. jr.: Role of fluid pressure in jointing, *Am. J. Sci.*, 263(October), 633–646, 1965.

1042 Stenhouse, P.: *Reactive Transport and Fluid Pathways in Fracture-Controlled Flow Systems*, (Doctoral
1043 Dissertation), Australian National University., 2014.

1044 Sweeney, J. J. and Burnham, A. K.: Evaluation of a Simple Model of Vitrinite Reflectance Based on Chemical
1045 Kinetics, *Am. Assoc. Pet. Geol. Bull.*, 74(10), 1559–1570, 1990.

1046 Teichmüller, R. and Teichmüller, M.: Relations between coalification and palaeogeothermics in Variscan and
1047 Alpidic foredeeps of western Europe, *Lect. Notes Earth Sci.*, 5, 1986.

1048 Terken, J. M. J.: The Natih petroleum system of north Oman, *GeoArabia*, 4(2), 157–180, 1999.

1049 Terken, J. M. J., Frewin, N. L., Indrelid, S. L. and Indrelin, S. L.: Petroleum systems of Oman: Charge timing and
1050 risks, *Am. Assoc. Pet. Geol. Bull.*, 85(10), 1817–1845, 2001.

1051 Vahrenkamp, V. C.: Chemostratigraphy of the Lower Cretaceous Shu'aiba Formation: A delta-13C reference
1052 profile for the Aptian Stage from the southern Neo-Tethys Ocean, *GeoArabia*, 1, 107–137, 2010.

1053 Velde, B. and Lanson, B.: Comparison of I/S transformation and maturity of organic matter at elevated
1054 temperatures, *Clays Clay Miner.*, 41(2), 178–183, 1993.

1055 Vermeesch, P.: How many grains are needed for a provenance study?, *Earth Planet. Sci. Lett.*, 224(3–4), 441–
1056 451, doi:10.1016/J.EPSL.2004.05.037, 2004.

1057 Virgo, S.: *Aspects of crack-seal vein system evolution*. (Doctoral Dissertation). Retrieved from [http://nbn-](http://nbn-resolving.de/urn/resolver.pl?urn=urn:nbn:de:hbz:82-opus-33858)
1058 [resolving.de/urn/resolver.pl?urn=urn:nbn:de:hbz:82-opus-33858](http://nbn-resolving.de/urn/resolver.pl?urn=urn:nbn:de:hbz:82-opus-33858)., RWTH Aachen University., 2015.

1059 Virgo, S. and Arndt, M.: Evolution of a crack-seal calcite vein network in limestone: a high resolution structural,
1060 microstructural and geochemical study from the Jebel Akhdar high pressure cell, Oman Mountains, (Diploma
1061 Thesis), RWTH Aachen [online] Available from: <http://darwin.bth.rwth-aachen.de/opus3/volltexte/2010/3385/>,
1062 2010.

1063 Virgo, S., Arndt, M., Sobisch, Z. Z. and Urai, J. L.: Development of fault and vein networks in a carbonate
1064 sequence near Hayl al-Shaz, Oman Mountains, *GeoArabia*, 18(2), 99–136 [online] Available from:
1065 <http://www.gulfpetrolink.net/publication/vol18.php>, 2013a.

1066 Virgo, S., Abe, S. and Urai, J. L.: Extension fracture propagation in rocks with veins: Insight into the crack-seal
1067 process using Discrete Element Method modeling, *J. Geophys. Res. Solid Earth*, 118(10), 5236–5251,
1068 doi:10.1002/2013JB010540, 2013b.

1069 Visser, W.: Burial and thermal history of Proterozoic source rocks in Oman, *Precambrian Res.*, 54(1), 15–36,
1070 doi:10.1016/0301-9268(91)90066-J, 1991.

1071 Warburton, J., Burnhill, T. J., Graham, R. H. and Isaac, K. P.: The evolution of the Oman Mountains Foreland
1072 Basin, *Geol. Soc. London, Spec. Publ.*, 49(1), 419–427, doi:10.1144/GSL.SP.1992.049.01.26, 1990.

1073 Warren, C. J., Parrish, R. R., Searle, M. P. and Waters, D. J.: Dating the subduction of the Arabian continental
1074 margin beneath the Semail ophiolite, Oman, *Geology*, 31(10), 889, doi:10.1130/G19666.1, 2003.

1075 Warren, C. J., Parrish, R. R., Waters, D. J. and Searle, M. P.: Dating the geologic history of Oman's Semail
1076 ophiolite: insights from U-Pb geochronology, *Contrib. to Mineral. Petrol.*, 150(4), 403–422, doi:10.1007/s00410-
1077 005-0028-5, 2005.

1078 Wygrala, B. P.: Integrated study on an oil field in the southern po basin, northern italy, *Berichte der*

1079 Kernforschungsanlage Jülich, 2313(October), 217, 1989.

1080

1081